

UNIVERSITÀ DEGLI STUDI DI BERGAMO

---

DIPARTIMENTO DI INGEGNERIA E SCIENZE APPLICATE

HIGHLY INTEGRATED WIRELESS MOTION SENSOR AND  
BIDIRECTIONAL INDUCTIVE CHARGERS FOR THE INTERNET OF  
THINGS ERA

*Tutor:*

Chiar.mo Prof.  
VALERIO RE

*Tesi di:*

MICHAEL GALIZZI

*Coordinatore del Dottorato:*

Chiar.mo Prof.  
MARCO SAVINI

---

Anno Accademico 2015/2016



*To my dad,  
the highlander*



# Contents

<b>Introduction</b>	<b>1</b>
<b>1 State of the Art</b>	<b>3</b>
1.1 State of the art in IoT wearable prototyping platforms . . . . .	3
1.1.1 STMicroelectronics BlueMicrosystem2 . . . . .	5
1.1.2 STMicroelectronics iNEMO-M1 . . . . .	6
1.1.3 STMicroelectronics WeSU . . . . .	8
1.1.4 Samsung ARTIK 020 . . . . .	8
1.1.5 Texas Instruments SensorTag . . . . .	9
1.1.6 Diolan SensiBLE . . . . .	10
1.1.7 NXP Hexiwear . . . . .	11
1.1.8 Thoughts regarding the state of the art in IoT development platforms	12
1.2 State of the art in Wireless Power Chargers . . . . .	13
<b>2 Wireless Motion Sensor Design</b>	<b>19</b>
2.1 Design . . . . .	21
2.1.1 Block Scheme . . . . .	21
2.1.2 Schematics . . . . .	24
2.1.3 Stackup . . . . .	28
2.1.4 Bluetooth RF antenna design . . . . .	28
2.1.5 Layout . . . . .	30
2.1.6 Antenna performance simulation . . . . .	32
2.2 Antenna Characterization . . . . .	33
2.2.1 Antenna Performance . . . . .	33
2.2.2 Pattern Emission . . . . .	33

2.2.3	Anechoic Chambers . . . . .	33
2.2.3.1	XY plane emission . . . . .	36
2.2.3.2	ZX plane emission . . . . .	37
2.2.3.3	ZY plane emission . . . . .	38
2.3	Android App Design . . . . .	39
2.4	Use Cases . . . . .	40
2.4.1	Use case 1: Door and Window Sensor . . . . .	40
2.4.1.1	Calibration procedure and angles learning . . . . .	40
2.4.1.2	Embedded firmware . . . . .	42
2.4.1.3	Android App for door sensor . . . . .	44
2.4.1.4	Validation of the system . . . . .	45
2.4.2	Use case 2: Synchronized body area network . . . . .	46
2.4.2.1	Central node . . . . .	46
2.4.2.2	Peripheral node . . . . .	47
2.4.2.3	Two central nodes BAN . . . . .	49
2.4.3	Use case 3: Beacon . . . . .	51
2.5	Conclusions . . . . .	53
<b>3</b>	<b>Wireless Power Charger Design</b>	<b>55</b>
3.1	Wireless Power Transmitter Module . . . . .	56
3.1.1	Block Scheme . . . . .	58
3.1.2	Schematics . . . . .	59
3.1.3	Layout . . . . .	62
3.1.4	Communication Unit . . . . .	64
3.1.5	Firmware Architecture . . . . .	66
3.1.6	Characterization . . . . .	68
3.2	Wireless Power Transmitter Evaluation kit . . . . .	69
3.2.1	Block Scheme . . . . .	70
3.2.2	Schematics . . . . .	72
3.2.3	Layout . . . . .	75
3.3	Wireless Power Receiver Module . . . . .	75
3.3.1	Block Scheme . . . . .	75
3.3.2	Schematics . . . . .	78

3.3.3	Layout . . . . .	80
3.3.4	Firmware structure . . . . .	82
3.4	Wireless Power Tx / Rx ASIC development . . . . .	82
3.4.1	PowerShare development . . . . .	84
3.4.2	Development on FPGA board . . . . .	84
3.4.2.1	Analog board development . . . . .	88
3.4.2.2	FPGA firmware development . . . . .	90
3.4.3	STWLC53 wireless power transmitter / receiver . . . . .	92
3.4.3.1	Transmitter mode . . . . .	92
3.4.3.2	Receiver mode . . . . .	93
3.4.4	Schematics of the STWLC53 evaluation board . . . . .	94
3.4.5	Communication Unit . . . . .	96
3.4.5.1	Analog watchdog . . . . .	97
3.4.6	Firmware . . . . .	99
3.4.7	Characterization in transmission mode . . . . .	99
3.4.7.1	Thermal performance . . . . .	99
3.4.7.2	Efficiency . . . . .	100
3.5	Conclusions . . . . .	101
3.5.1	Demonstration . . . . .	102
	<b>Conclusions</b>	<b>105</b>
	<b>Bibliography</b>	<b>107</b>



# List of Figures

1.1	BlueMicrosystem2 hardware setup . . . . .	5
1.2	ST iNEMO-M1 . . . . .	7
1.3	iNEMO-M1 discovery board . . . . .	7
1.4	WeSU platform . . . . .	8
1.5	ARTIK 020 BTLE Module . . . . .	9
1.6	TI SensorTag platform . . . . .	9
1.7	<i>SensiBLE</i> platform . . . . .	11
1.8	NXP Hexiwear . . . . .	11
1.9	Evaluation kit for wireless power charging transmitter by some semiconductor manufacturer . . . . .	16
1.10	Some evaluation kit for wireless power receivers proposed by some semiconductor manufacturer . . . . .	17
2.1	SensorTile kit image as shown on [STM16b]. The development kit includes the SensorTile module, the 100 mAh LiPO battery, the programming cable (SWD), a plastic case and two cradles for wearable application and development purpose. . . . .	20
2.2	Block scheme of the SensorTile board . . . . .	21
2.3	SensorTile main components and pinout, as shown in [STM16b] . . . . .	23
2.4	3D rendering of the <i>SensorTile</i> platform . . . . .	23
2.5	Bluetooth Low-Energy Section Schematic . . . . .	24
2.6	Motion Sensor, Environmental Sensor and Microphone Schematic . . . . .	25
2.7	Microcontroller and Oscillator Schematic . . . . .	26
2.8	Power Supply and External Connector Schematic . . . . .	27
2.9	PCB 3D Build up . . . . .	28

2.10	Microstrip line with signal ground plane. $W$ is the width gap between ground and signal line, $S$ the track width, $h$ is the thickness of the dielectric material and $\epsilon_r$ the relative dielectric constant. $L$ is the length of the signal line. . . . .	29
2.11	Antenna (ANT1) line feed details . . . . .	30
2.12	Four layer layout, top view, of the miniaturize wireless motion sensor . . . . .	31
2.13	Simulated <i>voltage standing wave ratio</i> (VSWR) and <i>efficiency</i> in the 2.4 GHz band (delimited in yellow). . . . .	32
2.14	Reference axes for pattern emission on XY, ZX and ZY planes . . . . .	34
2.15	Tapered anechoic chamber . . . . .	34
2.16	Near field anechoic chamber . . . . .	35
2.17	Rectangular anechoic chamber . . . . .	35
2.18	Radiation pattern @ 2.4 GHz with Horizontal Polarization (left image) and Vertical Polarization (right image) . . . . .	36
2.19	Radiation pattern @ 2.4 GHz with Horizontal Polarization (left image) and Vertical Polarization (right image) . . . . .	37
2.20	Radiation pattern @ 2.4 GHz with Horizontal Polarization (left image) and Vertical Polarization (right image) . . . . .	38
2.21	Android App example . . . . .	39
2.22	Magnetometer calibration procedure at power up . . . . .	40
2.23	<i>SensorTile</i> applied on a door . . . . .	41
2.24	Acceleration during the learning procedure. Spikes on the accelerometer are used to determine the angle when the door is closed. . . . .	42
2.25	Algorithm for door state identification . . . . .	42
2.26	Firmware flow-chart . . . . .	44
2.27	Android App for Door and Window sensor, running on an Android smartphone . . . . .	45
2.28	Validation of the algorithm. In blue the angle of the door and in red the status (opened or closed). . . . .	45
2.29	Simplified view of a Body Area Network . . . . .	47
2.30	Body Area Network example with 7 <i>Peripheral</i> nodes (to the left of the ruler), and one <i>Central</i> (to the right of the ruler) connected via USB to a PC . . . . .	48

2.31	Body Area Network estimated output data rates and offsets. In this case 7 <i>Peripherals</i> node are connected. This information are streamed out by the <i>Central</i> node to a PC via USB virtual COM port . . . . .	48
2.32	BAN with 16 <i>Peripherals</i> node and 2 <i>Centrals</i> (on the centre). The central nodes are connected to a PC via USB (blue and red cables) . . . . .	49
2.33	Streaming from two central nodes to a PC, via two USB Virtual COM ports	50
2.34	<i>SensorTile</i> used as Beacon. The App used on the Android device is Locate and can estimate the distance from the Beacon . . . . .	53
3.1	Qi standard block scheme of power receiver and power transmitter as reported in [Con] . . . . .	56
3.2	Block scheme of the STM32L1-based Wireless Power Transmitter board .	58
3.3	Microcontroller and power regulation section schematic . . . . .	59
3.4	High current bridge driver, power MOSFETs and tank resonator schematic	60
3.5	Current, voltage and temperature sense with one LED schematic . . . . .	61
3.6	3D rendering of the miniaturized Wireless Power Transmitter. The PCB form factor is only 13 mm X 13 mm size . . . . .	62
3.7	Four layer layout, top view, of the miniaturized wireless power transmitter	63
3.8	Photos of the miniaturized wireless power transmitter . . . . .	64
3.9	Power inverter and carrier demodulation section . . . . .	64
3.10	Block scheme of the digital demodulator block . . . . .	65
3.11	Firmware structure for discrete wireless power transmitter. The figure depicts the function call structure . . . . .	67
3.12	PWM power carrier during ping and transmission phase. The timing diagram shows that the Ping lasts for 90 ms and if no packet is modulated on that period, timeout occurs and the transmitter turns off the power carrier and return in stop mode for one second. If a packet is detected (modulation is present) during the ping phase, the power carrier is kept on, and a new timeout value is set to 500 ms in order to wait for the next packet. . . . .	68
3.13	Measured noise on USB power supply, AC coupled, due to switching activity of power MOSFETs. Spikes on 5 V USB power supply are in the range of 120 mV as reported in [AV15] . . . . .	68

3.14	Efficiency test performed from 0.5 W up to 3.5 W. The distance between the receiver and transmitter coils is within 2 mm . . . . .	69
3.15	Firmware architecture. The Wireless Power Transmitter library works using the Hardware Abstraction Layer libraries by ST and allows the library to be reused on a wide set of platform. . . . .	70
3.16	Block scheme of the STM32F0-based Wireless Power Transmitter evaluation platform . . . . .	70
3.17	Power regulation and connectors section schematic of Evaluation board of power transmitter . . . . .	72
3.18	Microcontroller and analog front-end for current sense and voltage envelope detection . . . . .	73
3.19	High current bridge driver, power MOSFETs and tank resonator schematic	74
3.20	Two layers layout and photography of the evaluation kit. As depicted in this images, the platform has been designed to easily modify the PCB and probe signals available on the board . . . . .	75
3.21	Block scheme of the STM8L-based Wireless Power Receiver board . . .	76
3.22	Top and bottom 3D rendering of the miniaturized Wireless Power Receiver	77
3.23	Microcontroller and power regulation section schematic . . . . .	78
3.24	High current bridge driver, power MOSFETs and tank resonator schematic	79
3.25	Four layer layout, top view, of the miniaturized wireless power receiver .	81
3.26	Photo of the miniaturized wireless power receiver . . . . .	81
3.27	Firmware structure for discrete wireless power receiver. The figure depicts the function call structure . . . . .	82
3.28	Prior Art block diagram of wireless battery chargers. As specified by the	83
3.29	<i>PowerShare</i> patent pending application block diagram . . . . .	84
3.30	Xilinx Virtex®-6 FPGA Evaluation Kit . . . . .	85
3.31	Boards used to emulate a ASIC system before starting with the silicon production. The setup is composed by a FPGA evaluation kit, a port expander to increase the number of FPGA I/O, an analog board with analog and power front-end and a power transmitter coil. . . . .	86

3.32	Board connection structure. The WPC Coil is connected to the analog board (that contains the power inverter section), in turn connected to the Xilinx XM105 that expands the FPGA Virtex 6 board. The FPGA emulates an ARM® Cortex®-M4 CPU whose code can be debugged with a standard serial wire debugger (SWD) interface . . . . .	87
3.33	FPGA’s analog to digital external front end with dedicated analog power supply . . . . .	88
3.34	Power inverter / Active rectifier with high current bridge driver and envelope peak detector with voltage buffer . . . . .	89
3.35	IAR Embedded Workbench IDE. The IAR is the IDE used to develop the firmware for both the FPGA system and the ASIC . . . . .	90
3.36	Modified firmware structure. The figure depicts the function call structure as in Figure 3.11. The difference between the STM32L1 wireless power transmitter and the FPGA/ASIC version are highlighted in red. . . . .	91
3.37	STWLC53 working modes. In red are depicted the enabled blocks. The green arrows show the energy path from/to the coil to/from the DC supply	93
3.38	STWLC53 evaluation board with a power transmitter coil (Würth Electronics 760308111) . . . . .	95
3.39	Schematics of the STWLC53 evaluation board . . . . .	95
3.40	External envelope detector . . . . .	96
3.41	Frequency response of the envelope filter on VS1 input pin of the STWLC53 chip. In solid blue line the magnitude while dotted line is the phase response of the demodulator filter . . . . .	97
3.42	STWLC53 internal ASK demodulation front end, simplified block diagram	98
3.43	Thermal photography of the evaluation board while transmitting 1.3 A @ 6 V power supply (7.8 W). The temperature in the center, where is soldered the STWLC53 chip is lower than 40°C. . . . .	99
3.44	Efficiency measurement in Transmitter and Receiver mode . . . . .	100
3.45	Concept of the patent-pending “PowerShare” . . . . .	101
3.46	A fully working demonstration of the <i>PowerShare</i> concept . . . . .	103



# Introduction

**D**riven by the consumer electronics industry, wearable devices are the fastest ramping consumer technology up to date sizing up opportunities for new players and venture capital investors. Such success allowed new startup companies come and growing, offering brand new interconnected devices to customers. As a result, millions of new devices are now connected to the internet and they upload a wide number of biometric and physiological parameters to the cloud.

This thesis work will describe the design and characterization of two technologies highly requested by the internet of thing market today: miniaturized wireless motion sensors for wearable application and wireless battery chargers. These two technologies seems to continue demand reference designs.

The first chapter of this thesis will briefly introduce an overview of the most successful wearable device sold so far, focusing in summarizing core functions frequently recurring on hardware design. A list of features and sensors required by customer will be summarized in order to address the design and the development of an innovative platform for the internet of things market. The chapter will also introduce wireless power charger platforms available on the market for rapid prototyping of both wireless power transmitter and receiver devices.

The second chapter introduce and describe the *SensorTile* platform. The aim of the *SensorTile* development is to provide a reference design platform condensing the most recurring features of the most successful IoT platforms created and available on the market so far. The chapter concludes with a section dedicated to the improvements achieved compare to the miniaturized state-of-the-art development platforms and illustrate some use cases developed using the *SensorTile* platform.

The third chapter will be related to the wireless battery recharge. In this chapter will describe the design, prototype and realization of reference design platforms for both power

transmitter and receiver, created with standard microcontrollers. The wireless battery recharge is one of the most attractive and innovative technology introduced in consumer electronics so far and recently an increasing number of devices are embedding this feature.

This final chapter will describe the hardware and firmware realization of both a wireless power transmitters and receivers made with discrete components and it will also introduce a new patent-pending concept in wireless battery chargers that has been called *PowerShare*. In the end of the chapter a dedicated ASIC, designed in STMicroelectronics, will be briefly described.

# Chapter 1

## State of the Art

### 1.1 State of the art in IoT wearable prototyping platforms

*T*he glaring success of wearable devices in the internet of things market is undeniable: millions of these devices are now proliferating the market proposing specific features to track, monitor, analyze, log and store acquired user data. Some of these wearable devices restricts its features to accurately count the number of daily steps, others are able to monitor and estimate the performed physical activity. Further expanding features of wearable devices, physiological parameter of human body such blood pressure and heart rate can be monitored, logged and uploaded to the cloud.

In this section some development boards widely used by big companies and small startup for prototyping their product in the Internet of Things context will be described. The platforms described have been chosen based on recurring features, such the presence of inertial sensors, environmental and/or optical sensors, a programmable microcontroller which can run user code and algorithms and radio connectivity, preferably the bluetooth low-energy V4.0 or newer. The possibility to use such development boards as a sensor hub usable as it is in final products as a solderable module has been taken into account too.

Platform	CPU	FPU	A	B	G	P	H	M	T	R	mm <sup>2</sup>	So
iNEMO-M1	M3	N	Y	Y	Y	N	N	N	N	N	13x13	Y
WeSU	M3	N	Y	Y	Y	Y	N	N	Y	Y	25x25	N
BlueMicrosystem2	M4	Y	Y	Y	Y	Y	Y	Y	Y	Y	80x70	N
ARTIK 020	M4	Y	N	N	N	N	N	N	N	Y	13x15	Y
SensiBLE	M4	Y	Y	Y	Y	Y	Y	Y	Y	Y	30x20	N
SensorTag	M3	N	Y	Y	Y	Y	Y	Y	Y	Y	42x32	N
Hexiwear	M4	Y	Y	Y	Y	Y	Y	Y	Y	Y	50x50	N
<i>Target</i>	<i>M4</i>	<i>Y</i>	<i>Y</i>	<i>Y</i>	<i>Y</i>	<i>Y</i>	<i>Y</i>	<i>Y</i>	<i>Y</i>	<i>Y</i>	<i>13.5x13.5</i>	<i>Y</i>

Table 1.2: Components on the IoT development platforms taken as a reference. Legend is: A (accelerometer), B (magnetometer), G (gyroscope), P (pressure), H (humidity), M (microphone), T (temperature) and R (radio connectivity). The last column (So) is the possibility to solder the platform as a Sensor Hub module.

Name	Manufacturer	Price (USD)
iNEMO-M1	ST	40
WeSU	ST	49
BlueMicrosystem2	ST	~ 42
ARTIK 020	Samsung	5.2
SensiBLE	Diolan	139
SensorTag	TI	29
NXP	Hexiwear	49
<i>Target</i>	<i>ST</i>	<i>&lt; 90</i>

Table 1.1: List of some development kit for the Internet of Things available from STMicroelectronics and the competitors

### 1.1.1 STMicroelectronics BlueMicrosystem2

NUCLEO platforms have been created by STMicroelectronics with the aim of creating standardized development platform with a common set of pinout compatible with the Arduino™ Uno boards. The NUCLEO boards are the official evaluation kit for STMicroelectronics STM32 microcontroller and these platform are available for every family of STM32 microcontroller. The NUCLEO boards are very simple evaluation boards and embeds only a microcontroller with the possibility to debug the firmware by using the embedded STLink debugger. A wide set of header pin are available on board to connect Arduino™ Uno compatible expansion board. The expansion board provided by STMicroelectronics comes with the Arduino™ Uno form factor too and are called X-NUCLEO.

There are a wide set of X-NUCLEO expansion boards available from STMicroelectronics embedding MEMS sensors, radio connectivity (Bluetooth, WiFi and sub-GHz), motor controller, USB controller and so on. The X-NUCLEO boards, as in the Arduino™ Uno way, can be stacked one above the other, creating a development platform with the exact set of functionality needed.

The power supply is usually provided by the NUCLEO platform on which the X-NUCLEO expansion boards are connected on, and the communication between the NUCLEO's microcontroller and the X-NUCLEO sensors is performed by means of shared communication buses, usually I2C.

For the Internet of Things context, STMicroelectronics creates three hardware setup which can be replicated by means of NUCLEO and a wide set of X-NUCLEO expansion boards. These hardware setup are called BlueMicrosystem1, BlueMicrosystem2 and BlueMicrosystem3. In this section the BlueMicrosystem2 will be described as a state-of-the-art in Internet of Thing developing platform because it includes processing capability, MEMS inertial sensors, environmental sensor and bluetooth low-energy radio connectivity which are common requirement in IoT. In detail, the BlueMicrosystem2 setup can be

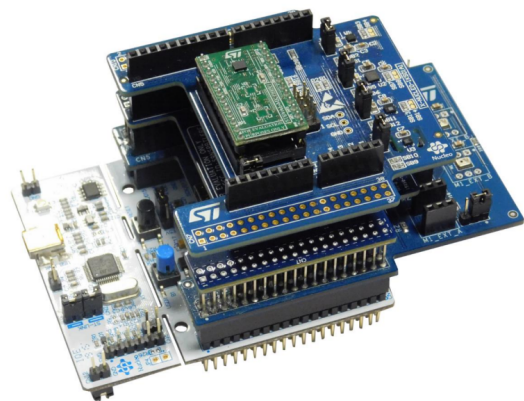


Figure 1.1: BlueMicrosystem2 hardware setup

achieved by interconnecting the following platforms:

- NUCLEO-F401RE or NUCLEO-L476RG that are development board which provide affordable and flexible prototyping with an Arduino™ Uno form factor.
- X-NUCLEO-IDB04A1, an expansion board including the BlueNRG-MS bluetooth low-energy radio chip
- X-NUCLEO-IKS01A1, a motion MEMS and environmental sensor expansion board
- X-NUCLEO-CCA02M1, an expansion board with a MP34DT01-M digital MEMS microphone

Moreover, the BlueMicrosystem2 hardware setup is enriched with a ready to use software package that can be used to evaluate the X-NUCLEO expansion board sensors and radio connectivity. The software package includes the firmware running on the NUCLEO board and Android and iOS app to test the bluetooth radio connectivity.

### 1.1.2 STMicroelectronics iNEMO-M1

Designed in 2012, the iNEMO-M1 is a system-on-board (SoB) 9-axis motion sensing platform in a tiny form factor. The iNEMO-M1 was designed to address requests from customer for a 9-axis sensor with processing capability able to provide an estimated orientation angle using geomagnetic information acquired from the sensors. The core of the iNEMO-M1 is a mainstream Cortex-M3 STM32F103REY6 microcontroller running at a frequency up to 72 MHz. The platform embeds two sensors:

- LSM303DLHC 6-axis digital e-compass module with accelerometer. The magnetometer has  $\pm 8.1$  gauss full scale range and the accelerometer has  $\pm 16g$  linear acceleration programmable full scale, as reported in the iNEMO-M1 datasheet [STM13]. The LSM303DLHC is considered an obsolete sensor and has been replaced by newer sensors by STMicroelectronics, for example the LSM303D.
- L3GD20 3-axis gyroscope with 2000 °/s of full scale manufactured with a CMOS / MEMS process developed by STMicroelectronics to produce inertial sensors and actuators on silicon wafers

The iNEMO-M1 platform is no longer recommended for new design due to the obsolescence of the components used in it. The microcontroller is a mainstream ARM Cortex-M3 with 72 MHz CPU and up to 512 Kbytes of Flash memory, but the lack of a Floating Point Unit acts as a bottleneck. Orientation estimation sensor fusion algorithms take advantages from the FPU, reducing drastically the execution time. Floating point libraries are available also for microcontroller without the FPU, but the power consumption and the execution time of algorithms could be up to ten times higher.

The iNEMO-M1 device provides a full set of serial communications such as I2C, SPI, UART and CAN bus which are very useful is the platform is used as a sensor hub. The iNEMO-M1 platform can be used as a central unit to process data acquired from embedded or external sensor and it is reusable as it is in a design because it comes in solderable, module-shaped PCB in a postage stamp size (13 mm x 13 mm) as shown in Figure 1.2.



Figure 1.2: ST iNEMO-M1

For evaluating the iNEMO-M1 module, a discovery platform is available for easily starting prototyping. The discovery platform, depicted in Figure 1.3, has the iNEMO-M1 platform in the center and connectors for communication and debugging purpose. The discovery board includes also a LPS331AP, a MEMS ambient pressure sensor connected on a I2C bus available on the iNEMO-M1 pin output.



Figure 1.3: iNEMO-M1 discovery board

Notwithstanding iNEMO-M1 has a full set of inertial sensors useful for orientation estimation, the lack of environmental sensor in the IoT context cannot be ignored. Moreover, radio connectivity is not embedded in this development platform and it can be achieved only by using external radio modules. The iNEMO-M1 system-on-board is no

longer recommended for new design and it has been replaced by system-on-chip solutions provided by STMicroelectronics.

### 1.1.3 STMicroelectronics WeSU

*WeSU* platform is a reference design *Wearable Sensor Unit*. It has been designed to help designers implement the latest technologies in wearable and portable applications, as reported in the data brief [STM16g].

*WeSU* development platform comes in a wearable form factor as depicted in Figure 1.4 and the size is about 30 mm X 23 mm and it is suitable for creating a bracelet for motion tracking analysis. The *WeSU* platform embeds an ultra low-power microcontroller STM32L1 which has the computational performance to estimate angles, altitude and run algorithms for activity recognition.

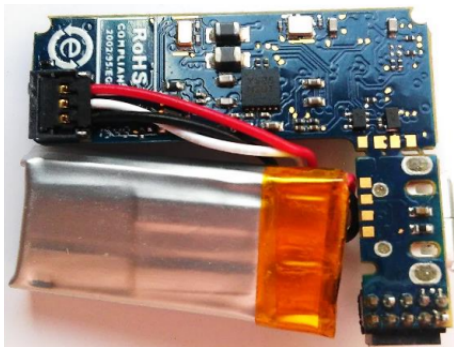


Figure 1.4: WeSU platform

The sensors embedded into the platform are 3D accelerometer with 3D gyroscope (LSM6DS3), a 3-axis magnetometer (LIS3MDL) and an environmental sensor to sense both temperature and pressure. Pressure sensor is the LPS25HB from STMicroelectronics featuring a very high resolution capable to sense variations in pressure of 0.01 hPa as reported in the Datasheet [STM16d], allowing the platforms to estimate the altitude and the vari-

ation with an accuracy of some centimeters. The *WeSU* platform is recommended for who want to start acquiring a wide set of data from the embedded sensors and developing algorithm based on the dataset. The wearable form factor, is also useful to start the design since Gerber design files are available on the STMicroelectronics website. The Bluetooth section has both IC and FCC certifications.

### 1.1.4 Samsung ARTIK 020

The ARTIK family chip from Samsung have been mainly designed to power the Internet of Thing market, as stated by Samsung. The ARTIK 020 chip is a simple Bluetooth 4.2 compliant module and does not embed any sensor, as reported in the product brief [Sam].

The ARTIK 020 module have standard peripherals commonly embedded into microcontrollers. Peripherals such as analog to digital converter, comparators, timers, serial buses and so on. The ARTIK 020 module is a solderable platform which comes in a small form factor of only 13 mm X 15 mm as depicted in Figure 1.5.



Figure 1.5: ARTIK 020 BTLE Module

### 1.1.5 Texas Instruments SensorTag

Design to demonstrate the potentiality of the Texas Instruments radio chip, the SensorTag is a development kit platform for the Internet of Thing environment and features a multi standard connectivity including Bluetooth Smart, 6LoWPAN and Zig-Bee. The SensorTag comes in a 50 mm X 67 mm PCB form factor as shown in Figure 1.6 and has a coin cell disposable battery on the bottom side for powering the platform. It embeds several inertial and geomagnetic sensors as well as optical and environmental sense capability.



Figure 1.6: TI SensorTag platform

- The 9-axis motion sensor provided by Invensense is the MPU-9250
  - The MPU-9250 is a MEMS MotionTracking™ device from Invensense which embeds two different chips, forming a System in Package device in a small form factor. The first device is a 6-axis (3-axis accelerometer plus a 3-axis

gyroscope) device with an on board digital motion processor capable of processing data acquired from the accelerometer and gyroscope, providing an embedded sensor fusion solution. The second chip embedded in the MPU-9250 is a 3-axis digital compass so that an attitude and heading reference system (AHRS) can be achieved

- A digital barometer BMP280 from Bosch Sensortec
  - The BMP280 absolute barometric pressure sensor is designed for mobile application and it exhibits an accuracy of  $\pm 0.12$  hPa, which means a resolution in altitude difference estimation of about 1 meter
- HDC1000 digital humidity sensor and TMP007 IR thermopile temperature sensor, from Texas Instruments
  - The TMP007 infrared temperature sensor is an integrated MEMS thermopile suitable for non-contact sensing and embeds an integrated math engine able to calculate the target voltage temperature based on the voltage across the thermopile
  - The HDC1000 is digital hygrometer sensor with an accuracy in relative humidity measurement of  $\pm 3\%$  and in ambient temperature measurement of  $\pm 0.2$  °C
- Digital microphone SPH0641LU from Knowles. The Knowles microphones are CMOS/MEMS technology platforms in a surface mount package

The SensorTag platform designed by Texas Instruments is a powerful tool to start new design and develop algorithm based on dataset acquired by the evaluation kit. The long lasting coin cell battery ensures the possibility to log data for long sessions, storing data into the embedded, 4 Mbit, serial Flash memory. The central unit beating into the SensorTag is a ultra low-power wireless microcontroller and can act as a Bluetooth Smart device, as ZigBee or 6LowPAN wireless network. The CPU capability is shared between the radio stack protocol and the user code.

### 1.1.6 Diolan SensiBLE

The Diolan *SensiBLE* is a small module, designed to be fully compatible with the BlueMicrosystem Open Development Environment (ODE) by STMicroelectronics. The *SensiBLE*, as reported on the datasheet [Dio], has been designed to provide the same functionality of the STMicroelectronics Nucleo components, in a wearable form factor. The form factor of the platform shown in Figure 1.7 measure 30 mm X 20 mm and is the key feature to help prototyping phase from the modularity of the ST Nucleo boards to the final device. It embeds a full set of geomagnetic, inertial and environmental sensors, covering a wide range of use cases. The Diolan *SensiBLE* it cannot be used as a solderable sensor hub, it can only be expanded using the two board-to-board connectors in Arduino style.

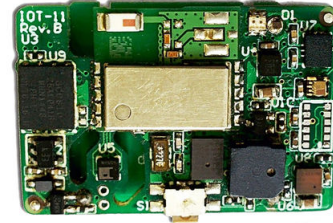


Figure 1.7: *SensiBLE* platform

### 1.1.7 NXP Hexiwear

The NXP silicon manufacturer proposed its own development platform for the Internet of Thing and called it Hexiwear. The NXP platform comes in a wearable form factor and it is completely open-source. Providing a easy access of data through the bluetooth low-energy communication this platform aim to simplify the development phases when NXP components have been choose in the design. The capability of stream a wealth of sensor data to a cloud make the Hexiwear a very attractive platform for the Internet of Thing simplifying the

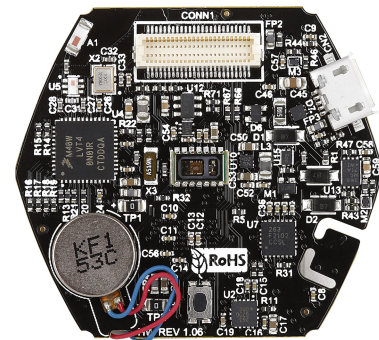


Figure 1.8: NXP Hexiwear

The Hexiwear hardware is designed around the ARM® Cortex®-M4 Kinetis K64\_120 microcontroller and embeds other devices from NXP such as:

- Bluetooth dual-mode connectivity by means of the KW40Z, an ARM® Cortex®-

M0+ Core radio microcontroller

- 9-axis inertial measurements, provided by two different sensors: a 3-axis digital gyroscope (FXAS21002C) and 3-axis accelerometer with 3-axis magnetometer ( embedded into a single chip, the FXOS8700CQ)
- Ambient pressure sensor measurement is performed with the MPL3115A2 which can read pressures from 20 to 110 kPa
- Battery charger is the MC34671 and can charge Li-Ion/Li-Polymer batteries with a current up to 600 mA

The Hexiwear is a complete IoT development solution and the main platform, depicted in Figure 1.8, can be further expanded by using the three sockets. Angle sensors, camera, CO sensors, GMS modules, hydrogen sensors, IR sensors, displays are only a subset of the features which can be added to the Hexiwear.

### **1.1.8 Thoughts regarding the state of the art in IoT development platforms**

Platform described in this section are boards designed by companies to provide a reference guide for designers are approaching new devices by a specific manufacturer. These development platforms usually come with a free software package ready to be modified in order to adapt the platform to their needs.

A common set of inertial and geomagnetic sensors are usually available, including an accelerometer, a magnetometer and a gyroscope. These very common set of sensors are useful when algorithms for motion tracking and activity recognition are implemented. For example, an attitude and heading reference system (AHRS) can be easily achieved. Environmental sensors such as temperature, pressure, humidity and light are very common sensors included in these platforms. Environmental sensors expand the capabilities allowing new features to be added. A pressure sensor, as an example, can be used both for weather forecasting or altitude estimation.

In IoT development a wide set of sensors is typically desirable to sense motions and the environment.

To process data acquired from sensors, these platforms embeds ultra low-power microcontrollers with a good computing performance. Cortex-M CPUs, designed by ARM and manufactured by several silicon manufacturers, are usually preferred. Connection of platform to the internet, for example to upload processed data to the cloud, is ensured typically by radio connectivity. The Bluetooth V4.0 Smart specification is the most common used technology for IoT because it ensure an extremely low power consumption with an acceptable throughput. Other radio technologies, such as Zigbee or WiFi can be used, but the implementation of the Bluetooth V4.0 low energy in most of the smartphones makes it the most preferred radio technology up to date.

## 1.2 State of the art in Wireless Power Chargers

This section will illustrate the state of the art of wireless power chargers, as it become a widely spread technology in consumer electronics. Wireless charging capability has been initially introduce to wirelessly recharge smartphone and the most common standards available was designed for low-power devices, with output power lower than 5 W. The most popular standard right now is Qi, defined by the Wireless Power Consortium (WPC). A rival called Powermat, under the Power Matters Alliance (PMA), now merged with the Alliance for Wireless Power (A4WP) to form the AirFuel™ Alliance, is pushing its new standard called Rezence.

Standards in wireless power chargers were born with the aim to harmonize the device architecture which want to use the wireless charging capability. The Qi standard, defined by the Wireless Power Consortium, is the most widespread in customer electronic up to now, but a great interest in PMA, and the new Rezence standard, is started few years ago.

There is no compatibility between standards because of some differences in hardware specs and in communication methods:

- Frequency range: Qi-compliant uses 110 kHz to 205 kHz, PMA-compliant uses 232 kHz to 278 kHz. Despite Qi and PMA standard work in a similar band, the A4WP uses a very different frequency (6.78 MHz)
- Power transfer: all systems are resonant, the difference is whether is choose to operate on-resonance (Rezence) or slightly off-resonance, as in Qi. The coupling be-

tween transmitter and receiver coil is tightly in Qi and PMA systems while A4WP systems are loosely coupled

- **Communication:** on both Qi and PMA standards the communication is in-band, with feedback signaling over the power path by means of the load modulation technique of power carrier. The A4WP communication path uses bluetooth low-energy technology with separate channels for power and control loop (out-of-band communication)
- **Efficiency:** the overall system efficiency in Qi and PMA is in the order of 70% or higher, while is it not specified the typical efficiency in A4WP. The Qi specification requires a minimum efficiency which must be achieved for different output powers. In case the efficiency drops below a minimum value, the power transfer phase has to be interrupted for safety reason
- **Spatial freedom:** PMA has the lowest spatial freedom whereas Qi standard could reach medium spatial freedom since multi coils topologies can be implemented. The A4WP has the highest spatial freedom because it uses loosely coupled coils

A brief list of wireless power transmitter and receiver chips implementing the standards described above are reported in Table 1.3. The Table 1.3 lists the family of ASICs developed by some semiconductor companies proposing their solution for wireless power charging implementation. Figure 1.9 shows Qi-compliant wireless power transmitter evaluation kit proposed as reference design by some semiconductor manufacturer.

This thesis work will focuses on the design of wireless power charger transmitter and receiver using standard microcontroller and avoiding the usage of dedicated and certified ASIC. Moreover, a section dedicated to the design of a novel ASIC with both wireless power transmitter and receiver functionality will be illustrated. The ASIC, called STWLC53, is also included in the Table 1.3 as per comparison with the competitor chip.

Manuf.	Name	Package	Function	P [W]	Standard
T.I.	BQ50xxxx	VQFN	Tx	5~15	Qi + PMA
T.I.	BQ51xxxx	DSBGA	Rx	2.5~10	Qi
ST	STWBC	VFQFPN32	Tx	5	Qi + PMA
ST	STWLCxx	Flip Chip	Rx	12	Qi + PMA
IDT	P9xxx	VFQFPN	Tx	3~7.5	Qi
IDT	P9xxx	WLCSP	Rx	3~15	Qi + PMA
Toshiba	TBxxxx	FN36, LQFP100	Tx	5~15	Qi
Toshiba	TCxxxx	WLCSP28	Rx	5~15	Qi
NXP	MWCT1xxx	32QFN, 64LQFP	Tx	5~15	Qi
NXP	MWPR1516	32QFN, 36WLCSP	Rx	15	Qi
Panasonic	NN32251A	HQFP64	Tx	5	Qi
Panasonic	AN32258A	XBGA048	Rx	5	Qi
ROHM	BD5702x	UQFN040V5050	Tx	5~15	Qi
ROHM	BD5701x	UCSP50L4C	Rx	5~10	Qi + PMA
<i>ST</i>	<i>STWLC53</i>	<i>52WLCSP</i>	<i>Tx / Rx</i>	<i>5 / 12</i>	<i>Qi + PMA</i>

Table 1.3: List of some Wireless Power Charger chip

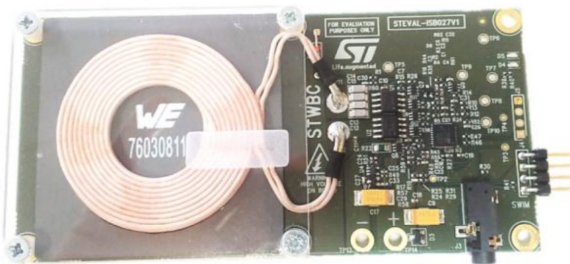
Evaluation kit for wireless power receiver chips are available and usually are designed on a PCB which aim to demonstrate the compactness of the proposed solution. Figure 1.10 depicts some wireless power receiver evaluation kit from ASIC manufacturer. Moreover, Figure 1.10c shows a very useful wireless power receiver, the AVID Qi Receiver Simulator, which is commonly used as a probe to test the functionality and the compliance of wireless power transmitters.



(a) NXP NXQ1TXH5DB1401



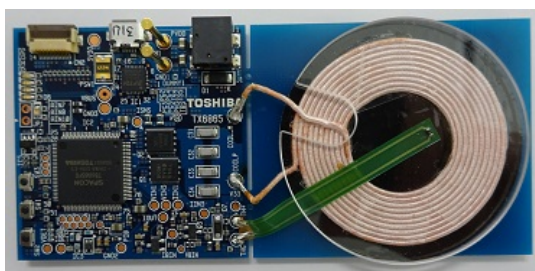
(b) Texas Instruments bq500212AEVM-550



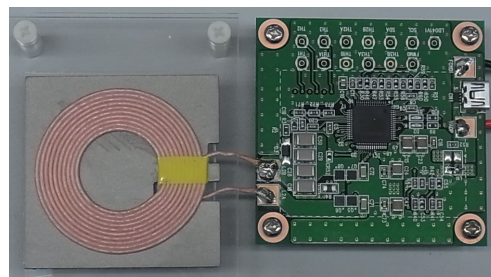
(c) STMicroelectronics STEVAL-ISB027V1



(d) IDT P9038-R-EVK



(e) Toshiba TB6865FG-EVM-001



(f) Panasonic NN32251 evaluation board

Figure 1.9: Evaluation kit for wireless power charging transmitter by some semiconductor manufacturer



(a) T.I. BQ51003EVM



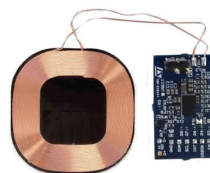
(b) ROHM / Würth receiver



(c) AVID Qi receiver simulator



(d) Panasonic receiver



(e) ST STWLC03

Figure 1.10: Some evaluation kit for wireless power receivers proposed by some semiconductor manufacturer



## Chapter 2

# Wireless Motion Sensor Design

*T*his chapter will illustrate the design, development, realization and characterization of a novel reference design platform for the STMicroelectronics IoT ecosystem, named *SensorTile*.

*SensorTile* is a Bluetooth low energy sensorized development kit. The miniaturized tile-shaped design includes all that is needed to remotely sense and measure motion, environmental and acoustical parameters. The board has been designed with a 9-DOF inertial measurement units (IMU), environmental (pressure, temperature and magnetic fields) sensors and a microphone. The onboard microcontroller is the STM32L476 ultra low power and offers enough power and processing capabilities to host MIPS intensive algorithms and user-defined application code.

The platform allows captured data to be transmitted through a Bluetooth Low Energy (BLE) connection, either by continuous streaming or by a convenient event notification mechanism – for instance, setting user-defined thresholds on monitored parameters.

The kit comes pre-configured to be immediately usable for evaluation enabling monitoring of parameters and simple programmability of event notifications through an Android or iOS Smartphone.

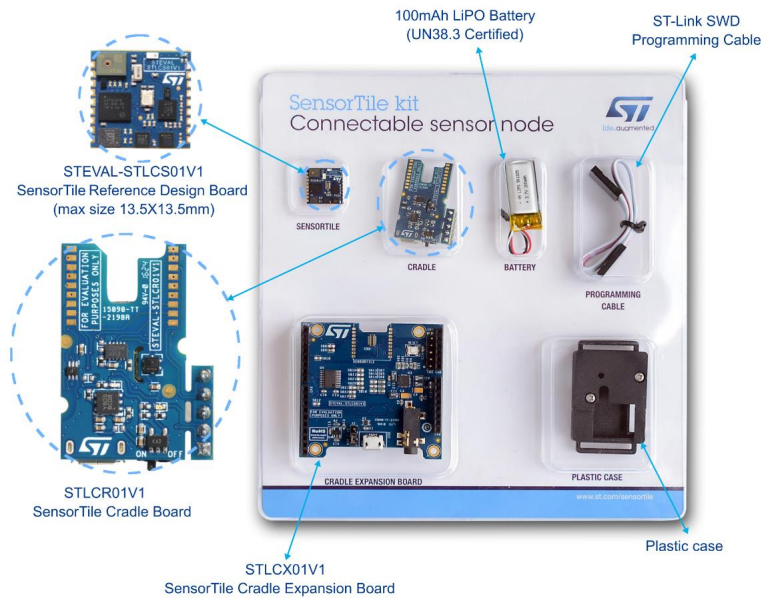


Figure 2.1: SensorTile kit image as shown on [STM16b]. The development kit includes the SensorTile module, the 100 mAh LiPO battery, the programming cable (SWD), a plastic case and two cradles for wearable application and development purpose.

Alternatively the kit can be used as a “sensor-and-connectivity hub” communicating with the main host processor via a simple serial protocol: this functional mode allows the designer to easily access sensor data and leverage on the BLE link without the hassle to read complex specifications or write time-consuming drivers. For more experienced users the SensorTile has a full-fledged software development kit (SDK) to enable rapid development of user-defined application code.

The SDK includes component drivers, BLE protocol stack with full-fledged profile suite and professional middleware libraries, such as 9-axis fusion and activity recognition engines (voice activity detection and other third-parties libraries will be added in future upgrades). To help developers jump start their designs it includes an attitude-and-heading-reference-system (AHRS) algorithm for orientation estimation. This chapter will be focused on design and characterization of the STEVAL-STLCS01V1 included into the SensorTile kit blister STEVAL-STLKT01V1 as shown in Figure 2.1.

## 2.1 Design

### 2.1.1 Block Scheme

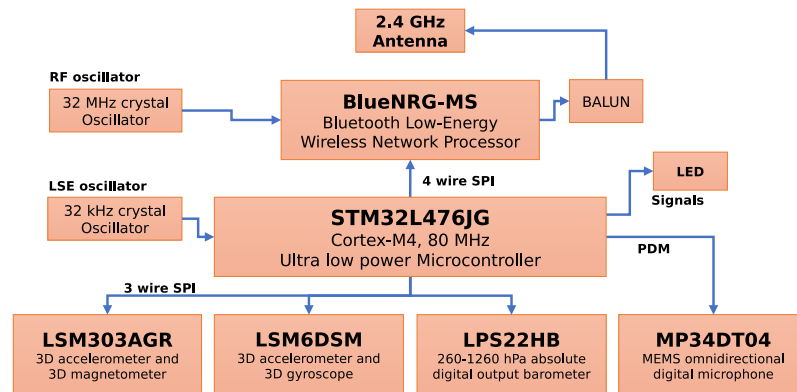


Figure 2.2: Block scheme of the SensorTile board

The SensorTile platform main components, with reference to Figure 2.3 are:

- (A) MP34DT04 [STM15b]: an ultra-compact, low-power, digital MEMS microphone built with a capacitive sensing element and PDM output format
- (B) LD39115J18R [STM14]: a 150 mA low quiescent current low noise 1.8 V voltage regulator with a typical dropout voltage of 80 mV and power supply rejection of 65 dB up to 10 kHz
- (C) STM32L476JGY6 [STM15c]: ultra-low-power ARM® Cortex®-M4 32-bit RISC microcontrollers operating up to 80 MHz with floating point unit (FPU) in single precision
- (D) LSM6DSM [STM16f]: is a system-in-package featuring a 3D digital accelerometer and a 3D digital gyroscope performing at 0.65 mA in high-performance mode. It has a full-scale acceleration range up to  $\pm 16$  g and an angular rate range up to  $\pm 2000$  dps
- (E) LSM303AGR [STM16e]: is an ultra-low-power high-performance system-in-package featuring a 3D digital linear acceleration sensor and a 3D digital magnetic

sensor. It has a full scales up to  $\pm 16g$  and a magnetic field dynamic range of  $\pm 50$  gauss

- (F) LPS22HB [STM16c]: is an ultra-compact piezoresistive absolute pressure sensor which functions as a digital output barometer
- (G) BLUENRG-MS [STM16a]: a very low power Bluetooth Low Energy (BLE) single-mode network processor, compliant with Bluetooth specification v4.1
- (H) BALF-NRG-01D3 [STM15a]: is the  $50\Omega$  conjugate match for the BlueNRG-MS chip, integrating balun transformer and harmonics filtering

#	Pin name	MCU pin	Main / alternative function
1	MIC_CLK	PC2	ADC_IN3, DFSDM_CKOUT
2	VDD_OUT	VDD/VBAT	1.8 V regulated output voltage
3	VIN	/	Power supply 2 V - 5.5 V
4	VDDUSB	VDDIO2/VDDUSB	USB Power supply 1.8 V - 3.3 V
5	GND	VSS	Ground
6	RXD/USBDP	PD2/PA12	USART5 RX or USB_OTG_FS DP
7	TXD/USBDM	PC12/PA11	USART5 TX or USB_OTG_FS DM
8	SAI_CLK	PG9	SAI2_SCK_A, SPI3_SCK
9	SAI_FS	PG10	SAI2_FS_A, SPI3_MISO
10	SAI_MCLK	PG11	SAI2_MCLK_A, SPI3_MOSI
11	SAI_SD	PG12	SAI2_SD_A, SPI3_NSS
12	GPIO2	PB8/PB9/PC1	DFSDM_DATIN6, I2C3_SDA
13	GPIO3	PC0	DFSDM_DATIN4, I2C3_SCL
14	NRST	NRST	STM32 Reset
15	SWD_CLK	PA14	SWD Programming interface clock
16	SWD_IO	PA13	SWD Programming interface IO
17	GND		Ground
18	GND		Ground

Table 2.1: Pinout description

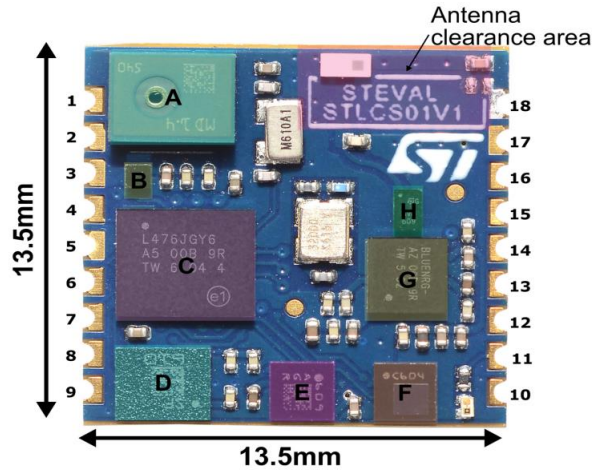
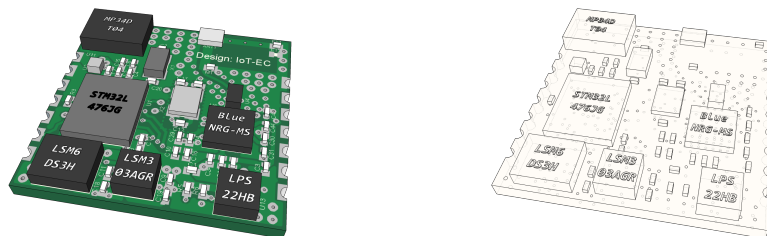


Figure 2.3: SensorTile main components and pinout, as shown in [STM16b]

A 3D rendering of the layout can be generated using a script available for Eagle Layout Editor. The script, called *eagleUp*, creates a Sketchup compatible file including 3D models of the components, if available. The script can also include textures on the generated 3D model, for example reproducing the routing of the PCB. The 3D model of the SensorTile platform can be used to have a better idea of the final size of the platform and it is very useful to start design a plastic enclosure which will contain the platform. Moreover, the 3D view of the platform provides a better feedback to a layout designer concerning components encumbrance which cannot be easily estimated using only a simple 2D view of the board.



(a) Top view 3D rendering

(b) SensorTile X-ray view, showing blind and through-hole vias

Figure 2.4: 3D rendering of the *SensorTile* platform

### 2.1.2 Schematics

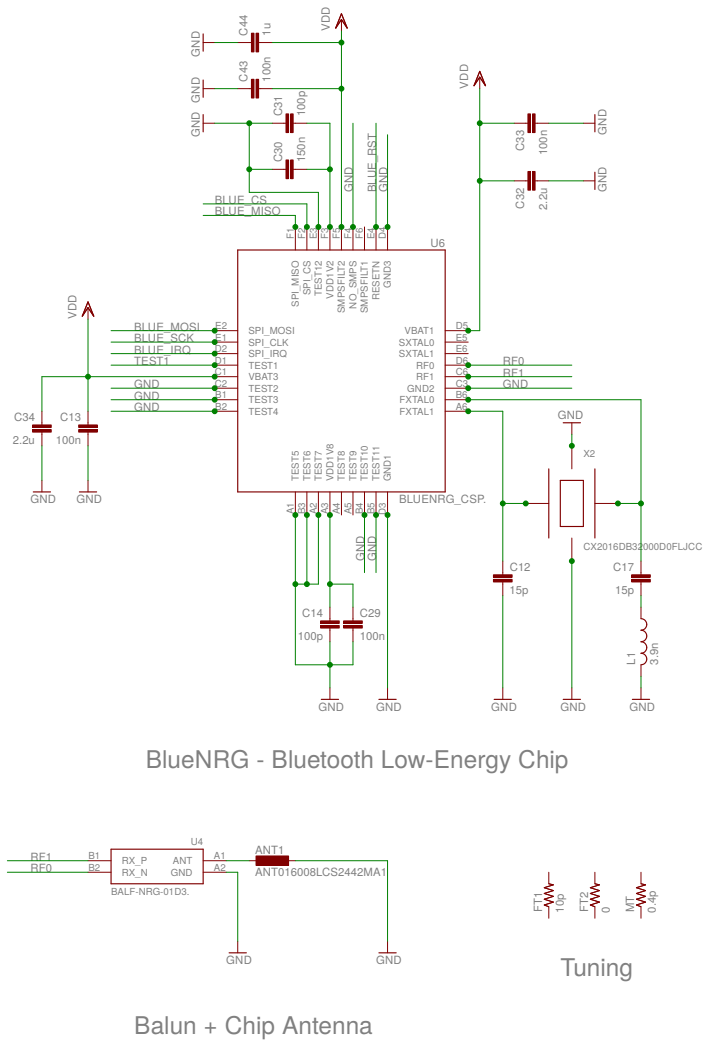


Figure 2.5: Bluetooth Low-Energy Section Schematic

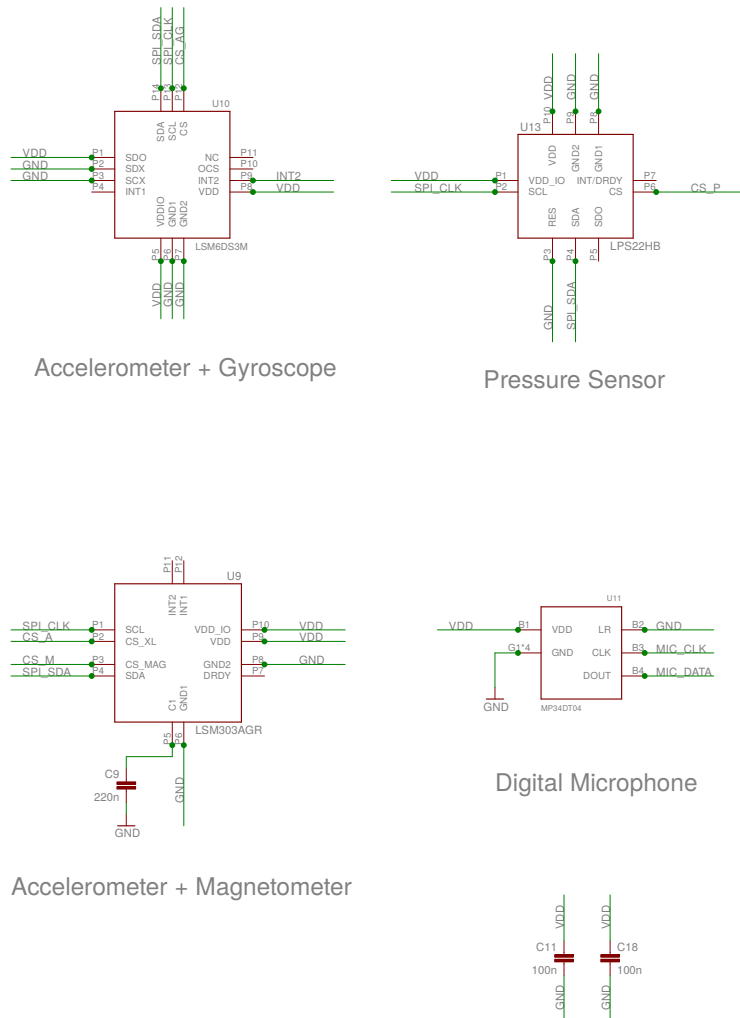
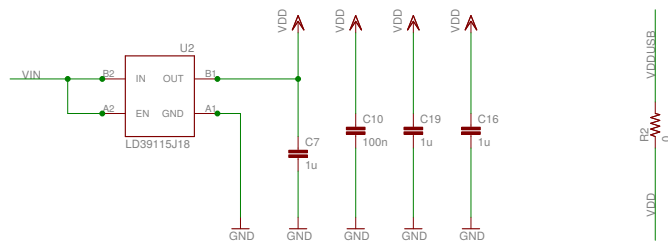
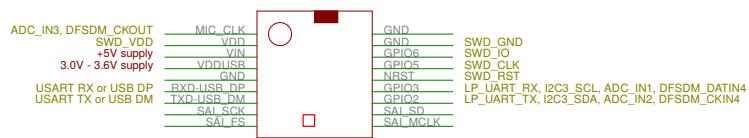


Figure 2.6: Motion Sensor, Environmental Sensor and Microphone Schematic

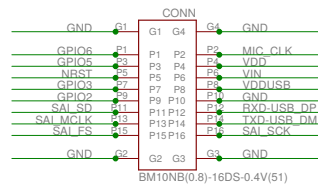




Low-Drop Out Voltage Regulator



Half-Moon Pin output



Hirose bottom connector (optional)

Figure 2.8: Power Supply and External Connector Schematic

### 2.1.3 Stackup

The stackup of the *SensorTile* has been designed in order to keep the mass production cost as low as possible. Due to the presence of 400  $\mu\text{m}$  pitch size WLCSP (wafer-level chip-scale package) components, which require blind vias to be routed, it was not possible to have a stackup with less than four layers. However, during the creation of the layout blind vias on the bottom layer have been avoided on purpose: in this way the PCB manufacturing cost has been significantly reduced. The overall stackup achieved for the *SensorTile* is depicted in Figure 2.9 and the thickness of the layer is listed in Table 2.2.

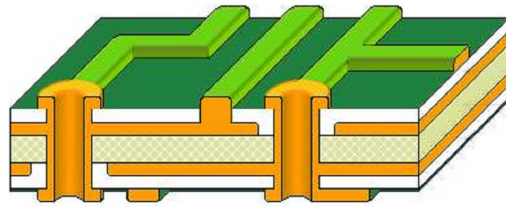


Figure 2.9: PCB 3D Build up

Layer	Thickness	Unit
L1	0.035	mm
Prepreg	0.1	mm
L2	0.035	mm
Core	0.7	mm
L3	0.035	mm
Prepreg	0.1	mm
L4	0.035	mm

Table 2.2: PCB Stack up thickness detail

### 2.1.4 Bluetooth RF antenna design

In this section the design and impedance matching calculation of the coplanar wave-guide with ground for the antenna line feed will be described.

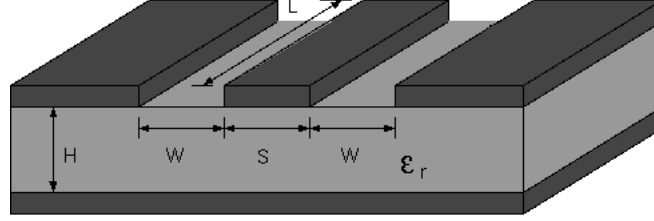


Figure 2.10: Microstrip line with signal ground plane.  $W$  is the width gap between ground and signal line,  $S$  the track width,  $h$  is the thickness of the dielectric material and  $\epsilon_r$  the relative dielectric constant.  $L$  is the length of the signal line.

The characteristic impedance  $Z_o$  of the feed microstrip with signal side ground plane can be calculated using 2.1 as reported in [Wad91].

$$Z_o = \frac{60.0\pi}{\sqrt{\epsilon_{eff}}} \frac{1.0}{\frac{K(k)}{K(k')} + \frac{K(kl)}{K(kl')}} \quad (2.1)$$

where, considering figure 2.10:

$$k = \frac{S}{2W + S} \quad kl = \frac{\tanh\left(\frac{\pi S}{4.0h}\right)}{\tanh\left(\frac{\pi(2W+S)}{4.0h}\right)}$$

$$k' = \sqrt{1.0 - k^2} \quad kl' = \sqrt{1.0 - kl^2}$$

and the effective dielectric value of the FR-4 PCB material between the top layer (feed line) and the second layer (reference ground for the antenna feed line) can be estimated by using the formula 2.2.

$$\epsilon_{eff} = \frac{1.0 + \epsilon_r \frac{K(k')}{K(k)} \frac{K(kl)}{K(kl')}}{1.0 + \frac{K(k')}{K(k)} \frac{K(kl)}{K(kl')}} \quad (2.2)$$

The  $K()$  in 2.1 and in 2.2 is the Elliptical Integrals of the First Kind as reported in [Mil87].

Considering the stackup of table 2.2, the thickness of the Prepreg material between layer 1 (feed line) and the layer 2 (reference ground plane) is 100  $\mu\text{m}$ . To obtain a perfect line matching of  $Z_o = 50 \Omega$  the track width must be 170  $\mu\text{m}$  as depicted in Figure 2.11.

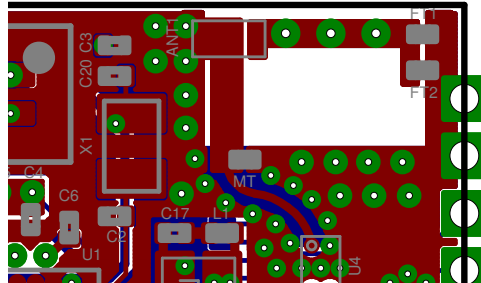


Figure 2.11: Antenna (ANT1) line feed details

For the sake of better understanding the feed line of Figure 2.11 is the red line from the U4 (the BALUN) component that reach the matching component MT. The track has  $170\ \mu\text{m}$  width and a ground aperture spacing of  $220\ \mu\text{m}$ . The position of the antenna is in the upper right corner of the PCB as depicted in Figure 2.12a thus enhancing the antenna gain as much as possible.

### 2.1.5 Layout

Layout of the module has been created with CadSoft Eagle 7.6.0, a freeware electronic design automation (EDA) application with a very powerful printed circuit board layout editor. The PCB of the *SensorTile* platform measures only  $13.5\ \text{mm} \times 13.5\ \text{mm}$  and has both a bottom connector and half-moon pins on two sides as shown in Figure 2.3. The connector on the bottom side allows the platform to be plugged without any soldering procedure, conversely the half-moon pins on the two sides allows the platform to be soldered as a module.

The positioning of the components on the *SensorTile* has been carefully addressed, in particular:

1. The magnetometer has been place away from high current traces, and there is an aperture in the ground plane below of its footprint. This expedients are mandatory to avoid distortions of the earth magnetic field measurement.

2. Bluetooth section has been properly designed to ensure the maximum efficiency in wireless communication. Despite the PCB size does not allow a free positioning of the bluetooth chip components, the placements has been made in order to guarantee the maximum compliance of design rules imposed by both the antenna manufacturer and the BlueNRG-MS chip constraint.

- (a) Concerning the antenna layout: the clearance and the aperture in ground plane has been respected as reported on the antenna datasheet [TDK16].
- (b) The PCB track which feed the antenna has been designed to meet the requirement of the  $50 \Omega$  controlled impedance; a better description of the feed track sizing has been described in Section 2.1.4.

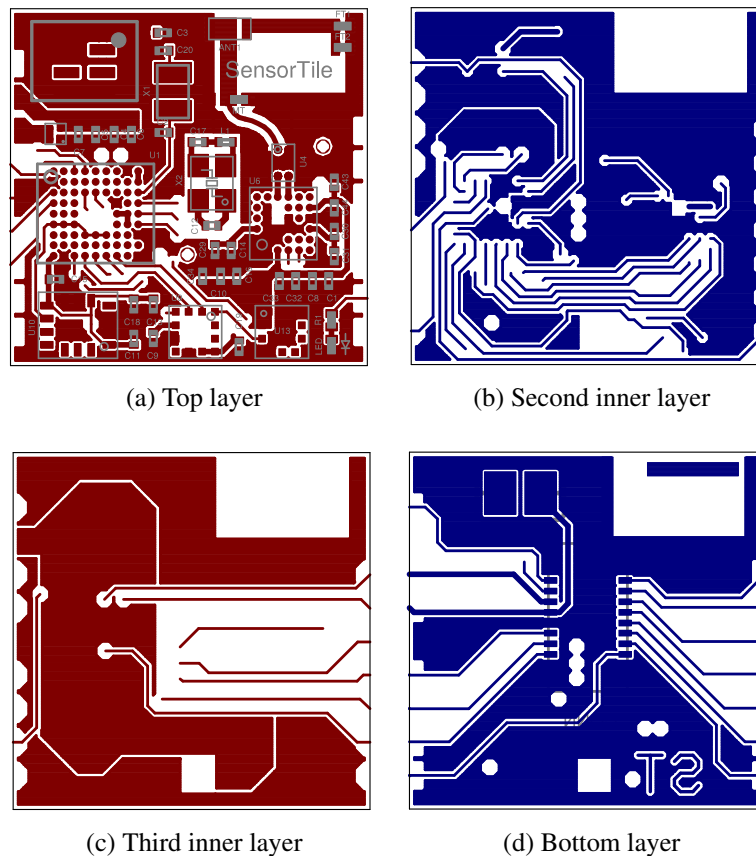


Figure 2.12: Four layer layout, top view, of the miniaturize wireless motion sensor

### 2.1.6 Antenna performance simulation

When the layout has been completed, some simulations of RF performance has been performed, in order to estimate some antenna performance. In RF antenna matching design the *reflection coefficient* and the antenna *efficiency* are considered. The voltage standing wave ratio (VSWR) can be estimated by simulation and the relation with the reflection coefficient is given by the formula 2.3, where  $\Gamma$  is the reflection coefficient.

$$VSWR = \frac{|V_{max}|}{|V_{min}|} = \frac{1 + |\Gamma|}{1 - |\Gamma|} \tag{2.3}$$

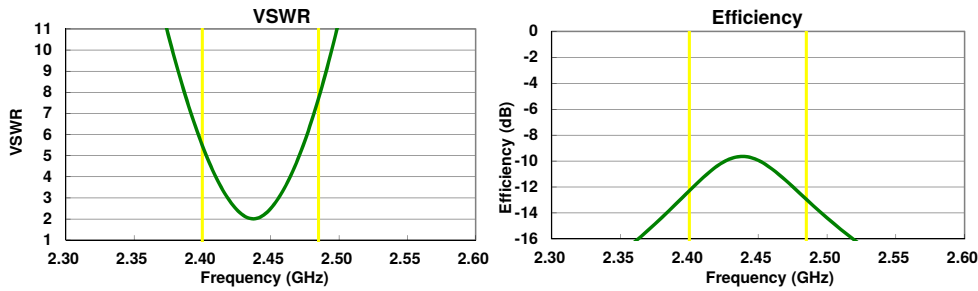


Figure 2.13: Simulated *voltage standing wave ratio* (VSWR) and *efficiency* in the 2.4 GHz band (delimited in yellow).

Frequency [GHz]	2.4	2.442	2.485
VSWR	5.5	2.09	7.7
Efficiency [dB]	-12.3	-9.7	-13

Table 2.3: VSWR and total antenna efficiency

Figure 2.13 depicts the simulated VSWR and the antenna efficiency in the 2.4 GHz band. As forecasted, even with a good antenna matching the expected efficiency will not be greater than 15%, because the size of the *SensorTile* board (and its ground plane) is smaller than the 2.4 GHz wave length (that is about 12.5 cm, while the *SensorTile* side is only 1.35 cm).

A good antenna matching in the SensorTile ensure the bluetooth chip do not overheat due to the signal reflection even if the overall antenna efficiency is not very high.

## 2.2 Antenna Characterization

In this section some performance analysis and pattern emission of the chip antenna will be presented. Antenna layout design in the 2.4 GHz domain is one of the most critical part of the layout design and must be carefully addressed to comply with the FCC declaration of conformity.

In the United States all electronic products must have a FCC certification which certifies that the electromagnetic interference of the manufactured device comply with the limits approved by the Federal Communication Commission (FCC). Any devices without an FCC certification can not be sold within the United States.

The designed SensorTile platform, as reported on [STM16b], accomplished the RF Test for FCC certification (FCC ID: S9NSTILE01) and IC certification (IC ID: 8976-STILE01).

### 2.2.1 Antenna Performance

### 2.2.2 Pattern Emission

Antennas are physical devices that radiate energy, frequently with some preferential directions. An antenna pattern emission is defined [Bal08] as a “graphical representation of the radiation properties of the antenna as a function of space coordinates”. If the antenna shows no preferential emission patterns it can be defined as isotropic.

In this section the measured radiation pattern in both *horizontal* and *vertical polarization* will be reported and illustrated on XY, ZX and ZY planes in order to compare the chip antenna emissions with an isotropic radiator having equal emissions in all directions [Bal08].

Reference axes of the module are depicted in Figure 2.14.

### 2.2.3 Anechoic Chambers

Tests have been performed in a *anechoic* (“*with no echo*”) *chamber*, that is a shielded room whose walls are covered with a material that absorbs most of the incident energy so

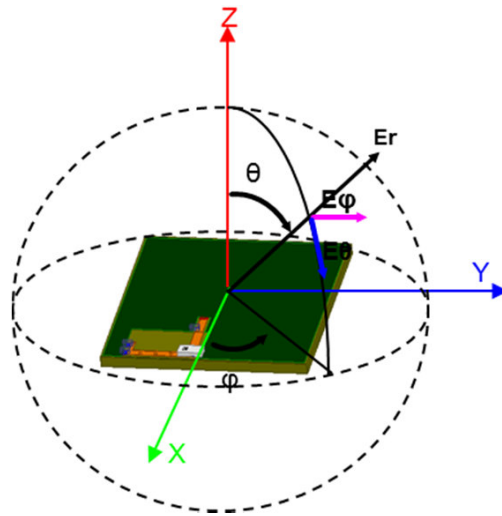


Figure 2.14: Reference axes for pattern emission on XY, ZX and ZY planes

that it can simulate free space. Most of the anechoic chamber used to perform antenna characterizations ensure an isolation performance in excess of 100 dB, preventing external signals polluting measurements.

The most common anechoic chambers are:

- Tapered anechoic chamber, shown in Figure 2.15: this kind of anechoic chambers are designed with one side of the chamber tapered. Tapering one side of the chamber causes the chamber to act like an indoor ground reflection range, forming an almost uniform plane wave at the test region. Frequency range are usually from 30 MHz up to 3 GHz

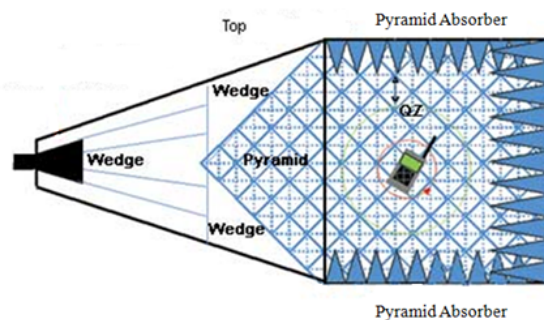


Figure 2.15: Tapered anechoic chamber

- Near field anechoic chamber, shown in Figure 2.16: in this kind of chamber, a cylindrical-shaped walls are used to measure the antenna radiation. With this chambers, only one plane at a time can be measured

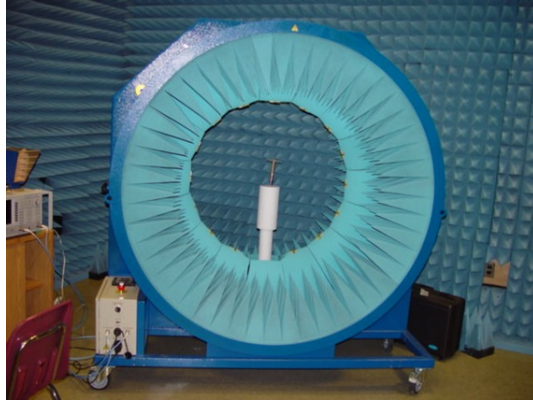


Figure 2.16: Near field anechoic chamber

- Rectangular chamber, shown in Figure 2.17: are the most used kind of chamber, because are easier to design and build compared to other anechoic chambers. The size of the chamber determines the range of the operating frequency

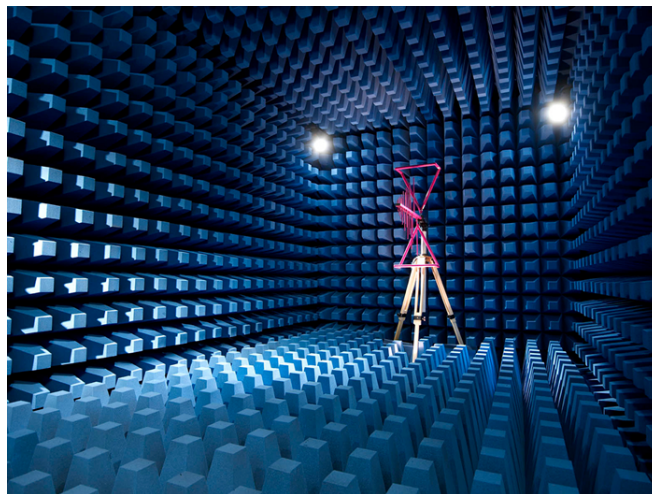


Figure 2.17: Rectangular anechoic chamber

2.2.3.1 XY plane emission

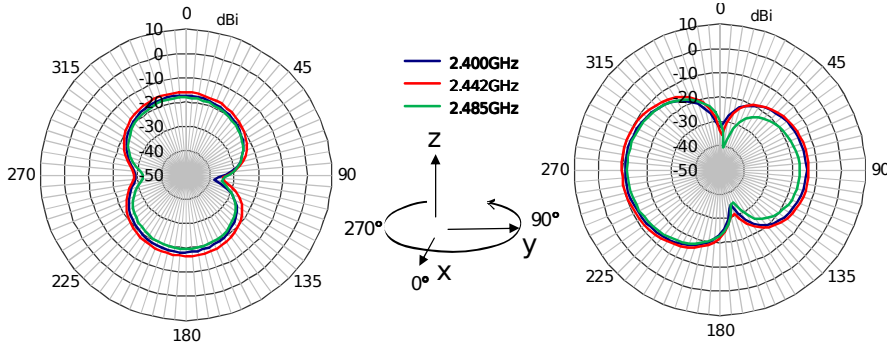


Figure 2.18: Radiation pattern @ 2.4 GHz with Horizontal Polarization (left image) and Vertical Polarization (right image)

The first measurement has been performed on the XY plane, considering both horizontal and vertical signal polarization. As described in Section 2.1.6 and depicted in Figure 2.13, the antenna efficiency cannot be higher than -10 dBi, because of the very limited size of the ground plane which is shorter than the RF wavelength. The simulated efficiency is furthermore confirmed by the measurements performed on the antenna. As depicted in Figures 2.18, 2.19 and 2.20, the measured efficiency is lower than -10 dB in all circumstances, for every orientation and for both horizontal and vertical polarization of the signal. Moreover, the pattern emission illustrated in Figures 2.18, 2.19 and 2.20 highlights the non omni-directionality of the chip antenna, as expected.

Freq [GHz]	2.4	2.442	2.485	Freq [GHz]	2.4	2.442	2.485
Avg [dBi]	-20.5	-19.0	-21.5	Avg [dBi]	-15.2	-14.0	-16.5
Max [dBi]	-17.2	-15.8	-18.0	Max [dBi]	-11.0	-9.6	-11.9
Min [dBi]	-38.2	-34.7	-35.0	Min [dBi]	-34.8	-35.2	-40.5

(a) Horizontal polarization

(b) Vertical polarization

Table 2.4: Output power on the XY plane

2.2.3.2 ZX plane emission

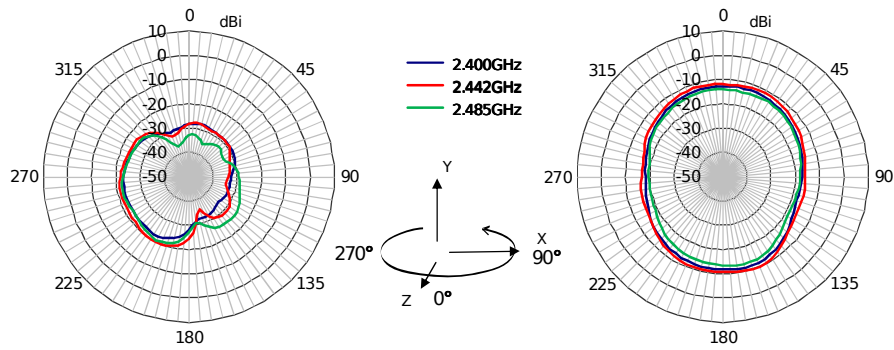


Figure 2.19: Radiation pattern @ 2.4 GHz with Horizontal Polarization (left image) and Vertical Polarization (right image)

As per the XY plane, the ZX plane radiation pattern measurements have been performed. The measurements are depicted in Figure 2.19 and the average, the maximum and the minimum value measured are reported in Table 2.5 for both horizontal and vertical polarization. The radiation pattern depicted in Figure 2.19 shows a better performance in vertical polarization compare to the horizontal polarization. The poor performance in horizontal polarization was definitely expected due to the perpendicularity of the signal with the very small ground plane.

Freq [GHz]	2.4	2.442	2.485	Freq [GHz]	2.4	2.442	2.485
Avg [dBi]	-26.4	-24.8	-25.7	Avg [dBi]	-14.1	-12.8	-15.5
Max [dBi]	-22.3	-19.6	-20.7	Max [dBi]	-11.5	-9.9	-12.9
Min [dBi]	-33.7	-36.0	-36.7	Min [dBi]	-18.1	-16.8	-19.6

(a) Horizontal polarization

(b) Vertical polarization

Table 2.5: Ouput power on the ZX plane

2.2.3.3 ZY plane emission

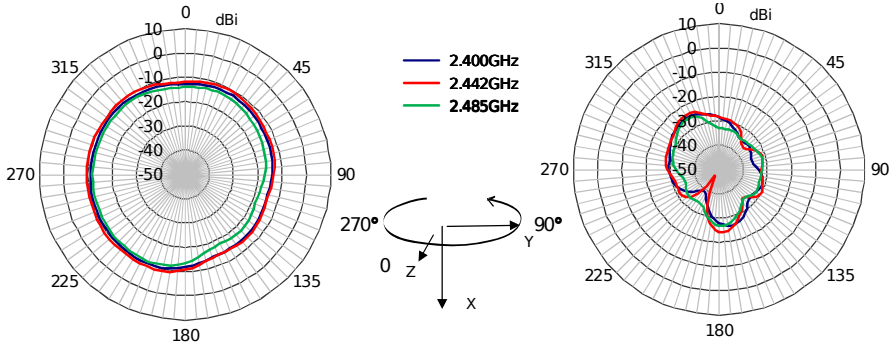


Figure 2.20: Radiation pattern @ 2.4 GHz with Horizontal Polarization (left image) and Vertical Polarization (right image)

On the ZY plane in horizontal and ZX plane in vertical polarization, as shown in Figures 2.19 and 2.20, the radiation pattern has the highest average gain in dBi. Such situation is common because the electromagnetic field is parallel to the wider side of ground plane of the *SensorTile*. A wide ground plane crossed by the electromagnetic field ensure a higher sensitivity in the antenna. Contrariwise the radiation emission is worse in ZY plane in vertical and ZX plane in horizontal polarization, because the ground plane crossed by the electromagnetic field has a negligible size.

For XY plane, in both horizontal and vertical polarization the antenna gain has a very high value, due to the same orientation of the ground plane with the EM field.

Freq [GHz]	2.4	2.442	2.485	Freq [GHz]	2.4	2.442	2.485
Avg [dBi]	-12.0	-10.9	-13.5	Avg [dBi]	-29.6	-28.8	-30.6
Max [dBi]	-10.1	-8.9	-11.1	Max [dBi]	-25.1	-23.7	-25.4
Min [dBi]	-14.9	-14.6	-18.6	Min [dBi]	-39.2	-46.7	-35.4

(a) Horizontal polarization

(b) Vertical polarization

Table 2.6: Ouput power on the ZY plane

## 2.3 Android App Design

- Main TAB: main tab includes an animated 3D parallelepiped which rotate accordingly with the orientation of the board, which stream out its estimated orientation. As depicted in Figure 2.21a a switch has been placed in order to activate the streaming from the platform. For completeness, both estimated angles (in degrees) and the linear acceleration is shown.
- The second TAB, depicted in Figure 2.21b, is dedicated to the magnetometer calibration. The gain matrix and the offset vector are both shown and are editable. Four buttons allow the user to reset the calibration parameters, write and read the value from and to the App. A recalibration button has been added also and allows the user to start a new calibration procedure.
- The third TAB contains some configuration of the platform. A radio button, as depicted in Figure 2.21c, is used to setup the streaming output datarate. Two buttons have been places to reset the estimated angles. RSSI estimated by the Android device where the App is running is also shown. In this TAB is also possible to enable some algorithms which run on board. The algorithms implemented are the activity recognition and the carry position.

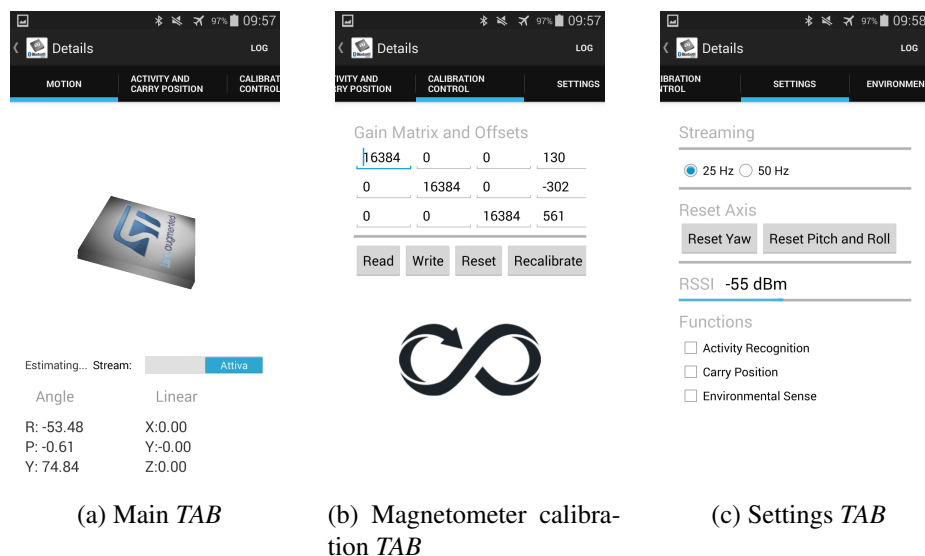


Figure 2.21: Android App example

## 2.4 Use Cases

In this section, some use cases of the *SensorTile* platform will be presented. As an example, two of most requested use cases have been implemented with the *SensorTile*, proving that a wide range of application can be fulfilled with this reference platform.

### 2.4.1 Use case 1: Door and Window Sensor

This section describes the realization of a door or window sensor for home security. The aim of this use case is to develop a specific firmware for the *SensorTile* platform and an Android App to monitor the output of the sensor.

#### 2.4.1.1 Calibration procedure and angles learning

When the *SensorTile* platform is powered up a magnetometer calibration is needed, specially if the magnetic environment changed. Despite the calibration parameters are stored into the microcontroller's non-volatile memory, whenever the platform is in a different magnetic environment this procedure becomes mandatory to achieve a correct behaviour of the embedded algorithms. The calibration procedure consists of a sequence of rotations of the platform around all axes, as depicted in Figure 2.22. Once the platform has accumulated enough data the amber LED on the platform blinks for 5 times, notifying that the calibration procedure has been successfully completed.

It is possible and highly suggested to continue this procedure for several times in order to increase the accuracy of the magnetometer calibration.

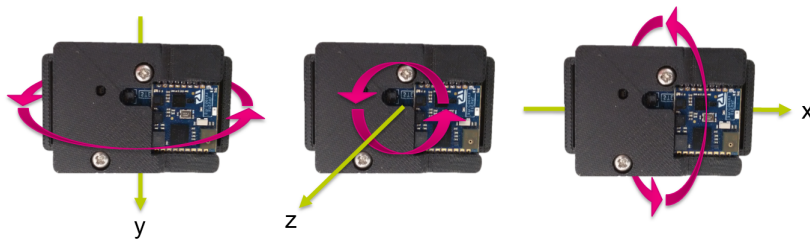


Figure 2.22: Magnetometer calibration procedure at power up

Once the magnetometer has been correctly calibrated, the platform can be applied on the door / window, trying to place it away from metallic objects (i.e.: the handle or the

lock). The orientation that must have the sensor applied on the door / window is shown in Figure 2.23.

The learning procedure consists of a series of opening / closing movements. The closing procedure determine a peak in the accelerometer, as depicted in Figure 2.24. The peak in the accelerometer is used to define the exact position in which the door has been effectively closed. A higher number of opening / closing trials increase the accuracy of the learned angle and significantly reduce the probability of false positive detections.



Figure 2.23: *SensorTile* applied on a door

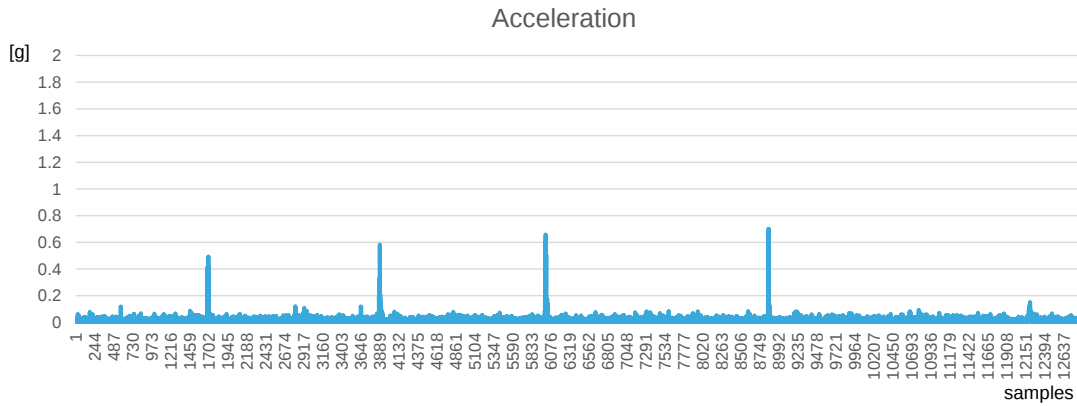


Figure 2.24: Acceleration during the learning procedure. Spikes on the accelerometer are used to determine the angle when the door is closed.

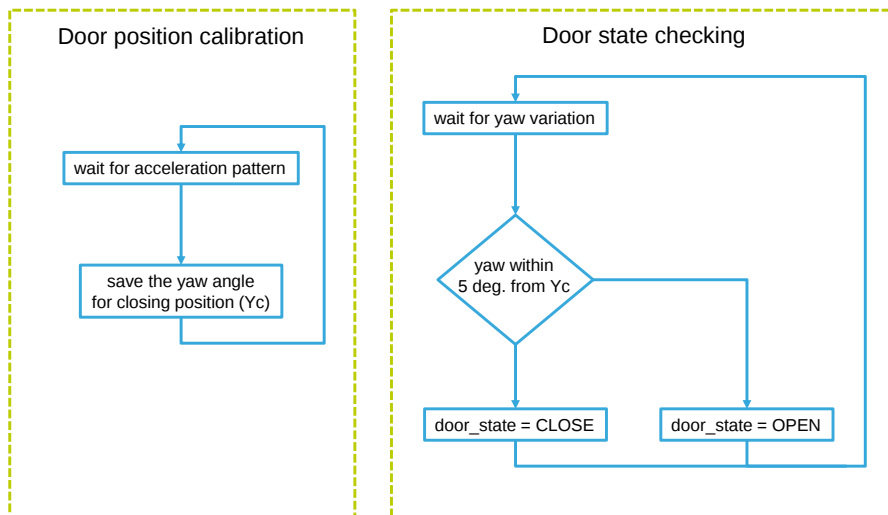


Figure 2.25: Algorithm for door state identification

### 2.4.1.2 Embedded firmware

The embedded firmware for the Door and Window sensor has been designed with the CubeMX hardware abstraction layer and the structure of the algorithm has been kept as simple as possible. An infinite loop performing sensor acquisition (from accelerometer and magnetometer) and execution of the OpenDoor algorithm at a fixed frequency has been implemented. The sensor used on the *SensorTile* platform to acquire the geomagnetic

information is the LSM303AGR, which integrates in a single chip both magnetometer and accelerometer. Both the sensor fusion (for Yaw angle estimation) and door state estimation algorithm runs at a frequency of 100 Hz instead of the Bluetooth low-energy streaming that run with an ODR of 10 Hz, to further reduce power consumption.

---

**Algorithm 1** Firmware main program file example

---

```
int main(void) {
    HAL_Init();
    SystemClock_Config();

    MX_GPIO_Init();
    MX_RTC_Init();
    MX_SPI1_Init();

    LSM303AGR_Configuration();
    compass_API_Init(0,0);
    compass_API_ForceReCalibration();
    IoT_OpenDoor_init(NULL);

    while (1) {

        LSM303AGR_ACC_Get_Acceleration(&spi1, Acceleration_mG);
        LSM303AGR_MAG_Get_Magnetic(&spi1, Magnetic_mGa);
        compass_API_SaveAcc(Acceleration_mG[0], Acceleration_mG[1], Acceleration_mG[2]);
        compass_API_SaveMag(Magnetic_mGa[0], Magnetic_mGa[1], Magnetic_mGa[2]);
        compass_API_Run();
        getCalibrationData(&calFactors);

        openDoor_input.acc[0] = (((float) Acceleration_mG[0]) / 1000);
        openDoor_input.acc[1] = -(((float) Acceleration_mG[2]) / 1000);
        openDoor_input.acc[2] = -(((float) Acceleration_mG[1]) / 1000);
        openDoor_input.mag[0] = ((float) (Magnetic_mGa[0] - calFactors.magOffX));
        openDoor_input.mag[1] = -((float) (Magnetic_mGa[2] - calFactors.magOffZ));
        openDoor_input.mag[2] = -((float) (Magnetic_mGa[1] - calFactors.magOffY));

        if ((calFactors.magOffX) || (calFactors.magOffY) || (calFactors.magOffZ)) {
            IoT_OpenDoor_run(&openDoor_input, &openDoor_output);
        }
        // Check if the door is open
        if (openDoor_output.event == 1) {
            // Handle the opened door event
        } else {
            // Handle the closed door event
        }
        HAL_Delay(10);
    }
}
```

---

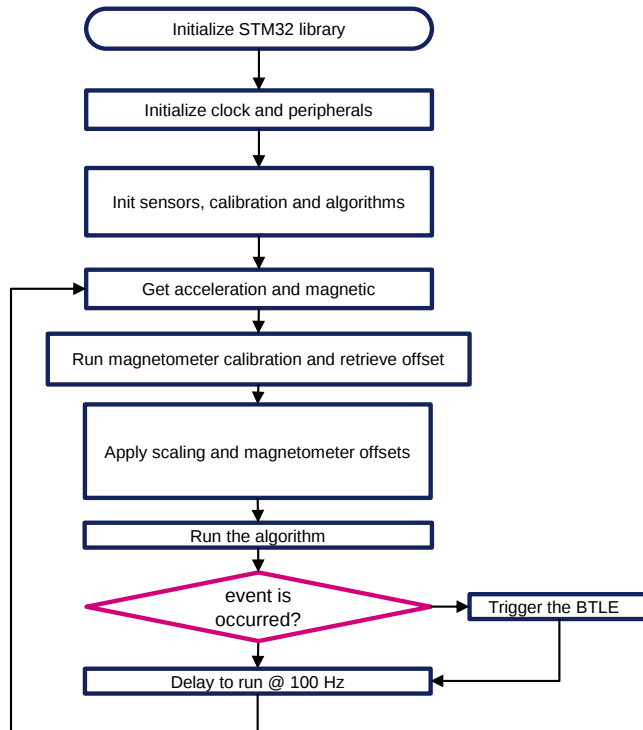


Figure 2.26: Firmware flow-chart

### 2.4.1.3 Android App for door sensor

An Android app has been created in order to perform some tests on the developed algorithm. The app is used to monitor and log the output of the algorithms and notify when the door is opened.

When the sensors are turned ON they become visible as “Security”, and can be connected. Once connected the App shows the status of the door (opened or closed) and if it is open it shows the Yaw angle of the door as well, as shown in screenshots of Figure 2.27.

Service	Characteristic	UUID	# of bytes	Descriptor
Security	Angle	128 bit	4 (float)	Notify
	Status	128 bit	1 (bool)	Notify

Table 2.7: Service and characteristics implemented on the SensorTile when used as Door or Window sensor

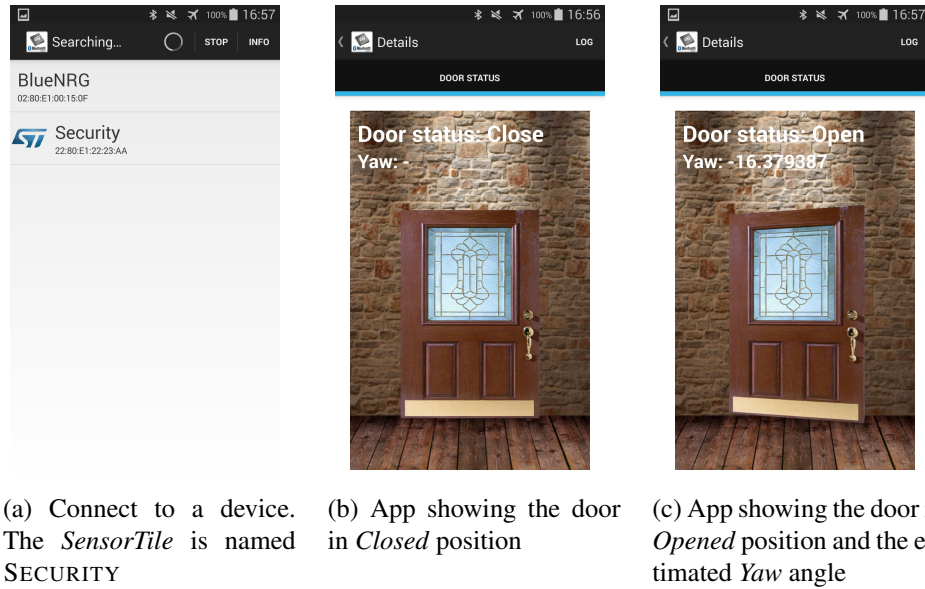


Figure 2.27: Android App for Door and Window sensor, running on an Android smartphone

#### 2.4.1.4 Validation of the system

To perform the validation of the door sensor created with the *SensorTile* platform, some opening/closing procedure have been performed. After a good magnetometer calibration, as described in Section 2.4.1.1, the sensor has been placed on a door and the result is depicted in Figure 2.28. The angle is estimated and the sensor fusion is able to correctly estimate the position of the door. The algorithm can also detect when the door is open (when the angle respect to a closed state is greater than 10 degrees).

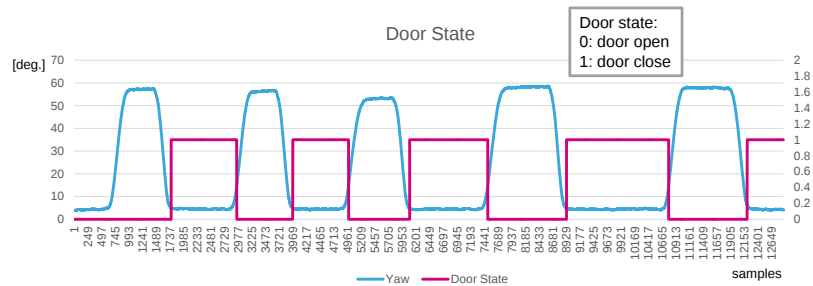


Figure 2.28: Validation of the algorithm. In blue the angle of the door and in red the status (opened or closed).

## 2.4.2 Use case 2: Synchronized body area network

Designed to address the problem of synchronisation of the sampling and streaming activity on wireless sensor nodes, the Body Area Network (BAN) has been developed to collect usable data from sensors located on a human body. The aim is to collect synchronized data in order to be able to determine a running, biking, sleeping activity. The timing and the synchronization is extremely important to accurately tracks movements. Synchronization ensures to have an accurate picture of what is happening at one point in time.

The Body Area Network has been developed with a set of worn sensor nodes (*Peripherals*), connected and synchronized with a master concentrator (*Central*) that collects the information from the nodes and redirect them on a remote device. Both *Peripherals* and *Central* nodes has been created with SensorTile platforms since the embedded Bluetooth Low-Energy chip support both master and slaves role. Unfortunately, despite Bluetooth low-energy is the leading radio technology for wearable sensors, this radio standard was never designed for network synchronization.

This use case design will address both the creation of a reliable Body Area Network with up to 8 *Peripherals* nodes per each *Central* and the synchronization of them with an acceptable tolerance.

### 2.4.2.1 Central node

From the *Central* node perspective, the tasks are:

1. Discovering available *Peripheral* nodes, based on the SSID name exposed by each node during advertising
2. Establishing a connection with a predefined number of nodes, with a maximum set of 8 *Peripherals*
3. Scanning the available services on each *Peripherals*
4. For each services, finds available characteristics and enable them for notification, if available

Once the Master node is connected to a set of *Peripherals* node, the streaming is started and the *Central* node begin to collect the incoming packets, estimating each node's output data

rate (ODR). The estimation is performed by counting and averaging the inter-arrival time between packets, and periodically (every 10 seconds), the ODR estimation is calculated on the *Central* node. Once the *Central* node has estimated the *Peripherals* ODR, this estimation is send back to the each individual nodes, that will recompute the drift from the target ODR and it adjusts the internal timer accordingly. The process of estimating the packets ODR in the *Central* node and changing the ODR on the *Peripherals* nodes is performed continuously and transparently from the user point of view. From the user's perspective, the initial ODR could be affected by a small drift from the selected ODR, but it will slowly converge to a perfect ODR match between nodes.

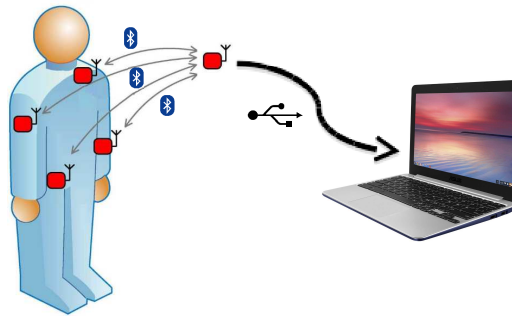


Figure 2.29: Simplified view of a Body Area Network

#### 2.4.2.2 Peripheral node

From the *Peripheral* node point of view, the following steps are performed on power up:

- The internal high-speed oscillator (HSI at 16 MHz) is calibrated using the low-speed external (LSE at 32.768 kHz as shown in Figure 2.7) crystal oscillator which have a 20 ppm deviation from the central frequency. Calibration of the internal oscillator allows to achieve 20 ppm deviation instead of the factory trimmed 1% deviation. This means:
  - With no calibration, the frequency deviation is up to: 160 kHz (1% of 16 MHz)
  - With calibration, the deviation can be lowered down to: 3.2 kHz (20 ppm at 16 MHz). The accuracy of the high-speed internal oscillator has been increased of

a factor of 50, having in this way a good starting point to further synchronize the peripherals ODR

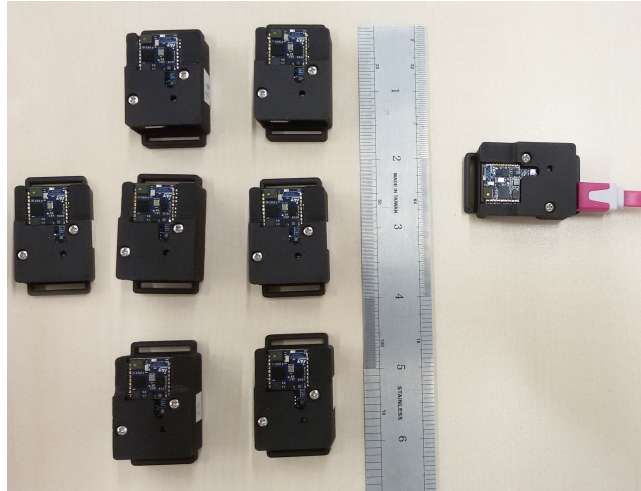


Figure 2.30: Body Area Network example with 7 *Peripheral* nodes (to the left of the ruler), and one *Central* (to the right of the ruler) connected via USB to a PC

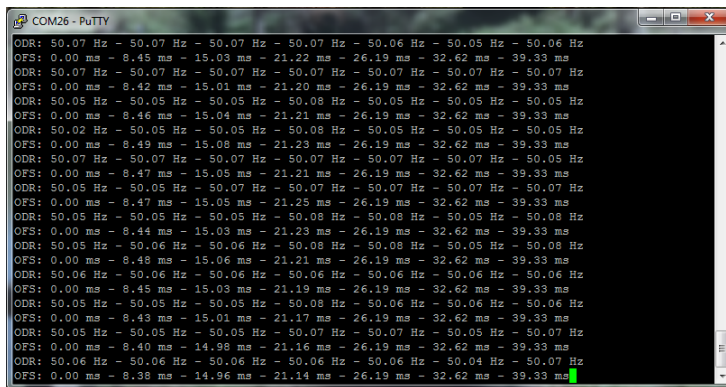


Figure 2.31: Body Area Network estimated output data rates and offsets. In this case 7 *Peripherals* node are connected. This information are streamed out by the *Central* node to a PC via USB virtual COM port

An example of Body Area Network (BAN) with 7 *Peripheral* nodes and one *Central* node is shown in Figure 2.30. The *Central* node of the Body Area Network is connected to a PC with a USB cable (in pink), and on the PC side is possible to log two kind of information, mutually exclusives:

1. Estimated output data rate and offset for each nodes (as shown in Figure 2.31)
2. Time-stamp and quaternion coming from each nodes (as shown in Figure 2.33)

In this case, for evaluate ODR synchronization, the ODR and offset are chosen to be logged, as depicted in Figure 2.31. The estimated ODR is 50 Hz for each nodes, with a maximum error of 0.07 Hz (that is less than 0.14% of ODR drift from desired value). The measured drift could be a measurement error instead of a real drift from the target ODR.

### 2.4.2.3 Two central nodes BAN

Bluetooth low-energy technology, by standard definition, allows one single *Central* node to handle an undefined number of connections simultaneously, however it is difficult to handle huge amount of connections on a single radio chip like the BlueNRG-MS, used in the *SensorTile* platform, due to hardware limitations. The BlueNRG-MS radio chip, in master mode, supports only 8 slave connections hence if we need more than 8 nodes for a Body Area Network we need to opt to a multi master network. Two *Central* nodes can handle up to 16 *Peripheral* nodes, without any contention from the radio point of view; Figure 2.32 shows a Body Area Network created with 2 central nodes, each of them connected to 8 *Peripherals* nodes streaming the estimated angle orientation at a output data rate of 50 Hz.

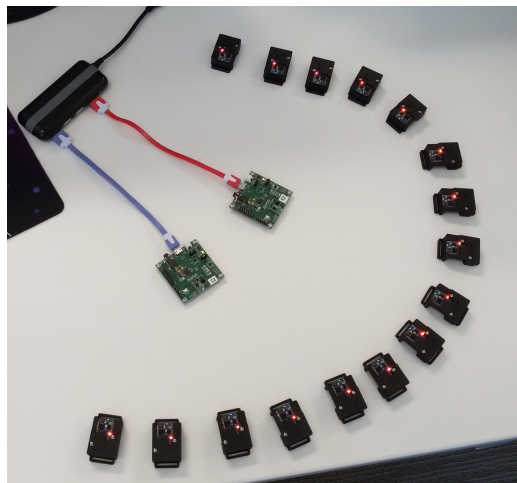


Figure 2.32: BAN with 16 *Peripherals* node and 2 *Centrals* (on the centre). The central nodes are connected to a PC via USB (blue and red cables)

In the current firmware, once *Centrals* boot up, they connects to 8 *Peripheral* devices, without any node preference, with a policy of “*first found, first connected*”. As a demonstration, in the two *Central* nodes of Figure 2.32 the connections have been arranged as depicted in Figure 2.33, id est:

- *Central #1* (on PC VCOM34) connected to *Peripherals* 11, 14, 10, 1, 15, 4, 16, 12.
- *Central #2* (on PC VCOM26) connected to *Peripherals* 8, 2, 9, 7, 3, 5, 13, 6.

The *Peripheral* nodes stream out data at a 50 Hz output data rate, but two packets are sent together in order to reduce the overall data rate. This mean, the effective over-the-air ODR is 25 Hz, though the sampled and received one is 50 Hz. Lets make some overall bandwidth estimation:

Each *Peripheral* packet is made of:

- Time-stamp, has 2 byte size (unsigned integer, 16 bit)
- Quaternion has 2 byte for each component (signed integer, 16 bit). For the sake of simplicity, only  $Q_X$ ,  $Q_Y$  and  $Q_Z$  components are sent, while  $Q_W$  is discarded (if  $Q_W$  is negative  $Q_X$ ,  $Q_Y$  and  $Q_Z$  are negated). In one *Peripheral* packet there are two quaternions, to double the ODR.

The size of a *Peripheral* packet is 14 bytes. Considering an ODR of 25 Hz, the throughput of a single node is 350 byte/s. If we take, as an example, the BAN with one *Central* node connected to 7 *Peripherals*, the total incoming throughput into the master node is up to 2.45 kbyte/s or rather 19.6 kbit/s.

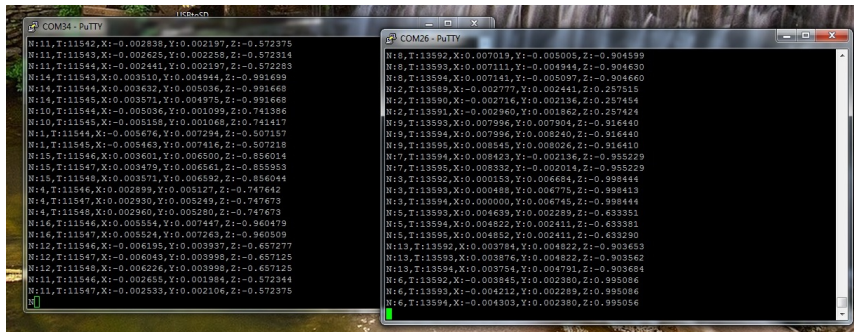


Figure 2.33: Streaming from two central nodes to a PC, via two USB Virtual COM ports

The Log file generated by the two *Centrals* are shown in Figure 2.33 where the node number, the time-stamp and the quaternions are listed.

### 2.4.3 Use case 3: Beacon

The Beacon is a bluetooth-based technology which allow devices to send and receive small messages in a short range. This protocol was developed by Apple and it was widely adopted by competitors in their bluetooth low-energy enabled devices. The protocol is very simple and consists of a bluetooth Beacon which broadcasts its identifier to nearby portable electronic devices. Bluetooth low-energy enabled devices in close proximity to the Beacon can perform action when receive broadcast messages.

With the Beacon broadcasted messages is possible to estimates the distance between the Beacon and the portable receiver device. The estimation can be performed by measuring the Received Signal Strength Indicator (RSSI) available on the receiver side.

To perform an accurate estimation of the distance, some preliminary calibrations are usually mandatory. As reported in [SB15], the distance  $d$  between the Beacon and a receiver can be estimated by using the Formula 2.4, where  $RSSI(d)$  is the signal strength measured at a distance  $d$  and  $RSSI(1m)$  is the signal strength measured at one meter. The Formula 2.4 must be calibrated using the Formula 2.5 where  $RSSI_x$  and  $RSSI_y$  are the signal strengths measured at a distance  $x$  and  $y$  (in meter, for example  $x=5 m$  and  $y=2 m$ ) respectively.

The function listed in Algorithm 2 shows the configuration of the BleNRG-MS chip to act as a Beacon device. The advertising data is a 26 byte packet containing some mandatory information used for beaconing, such as location UUID, major and minor number and the value of the transmitted power as specified by the Beacon protocol.

$$d = 10^{\frac{-RSSI(d)+RSSI(1m)}{10n}} \quad (2.4)$$

$$n = - \left( \frac{RSSI_x - RSSI_y}{10 \log_{10}(x - y)} \right) \quad (2.5)$$

---

**Algorithm 2** Function used to configure the BlueNRG-MS using an advertising packet structured as a Beacon

---

```

void Make_Discoverable(void) {
    tBleStatus ret = 0;
    uint16_t service_handle , dev_name_char_handle , appearance_char_handle;

    const uint8_t manuf_data[] = {
        26, AD_TYPE_MANUFACTURER_SPECIFIC_DATA, 0x4C, 0x00,
        0x02, // ID
        0x15, // Length of the remaining payload
        0xE2, 0x0A, 0x39, 0xF4, 0x73, 0xF5, 0x4B, 0xC4, // Location UUID
        0xA1, 0x2F, 0x17, 0xD1, 0xAD, 0x07, 0xA9, 0x61, 0x00, 0x00, // Major number
        0x00, 18, // Minor number
        0xC8 //2's complement of the Tx power (-56dB)};
    };

    // GATT Initialization
    ret += aci_gatt_init();

    // GAP Initialization
    ret += aci_gap_init(GAP_PERIPHERAL_ROLE, &service_handle ,
        &dev_name_char_handle , &appearance_char_handle);

    /* -2 dBm output power */
    ret += aci_hal_set_tx_power_level(0, 5);

    /* Disable scan response */
    hci_le_set_scan_resp_data(0, NULL);

    /* Put device in non connectable mode */
    ret += aci_gap_set_discoverable(ADV_NONCONN_IND, 1600, 1600, RANDOM_ADDR,
        NO_WHITE_LIST_USE, 0, NULL, 0, NULL, 0, 0);
    ret += aci_gap_delete_ad_type(AD_TYPE_TX_POWER_LEVEL);
    ret += aci_gap_update_adv_data(27, manuf_data);
}

```

---

The Figure 2.34 depicts the *SensorTile* while is in advertising as a Beacon, and a bluetooth low-energy enabled smartphone estimating the distance based on the *RSSI* and the Beacon advertising packet. The estimation performed on the smartphone is quite accurate (0.1 m is reported on the smartphone and it is the real distance between the devices as confirmed by the ruler).

The estimation of the distance can be performed simultaneously by multiple receiver devices because the devices are not connected when working in Beacon mode and advertising packets are always send in broadcast.

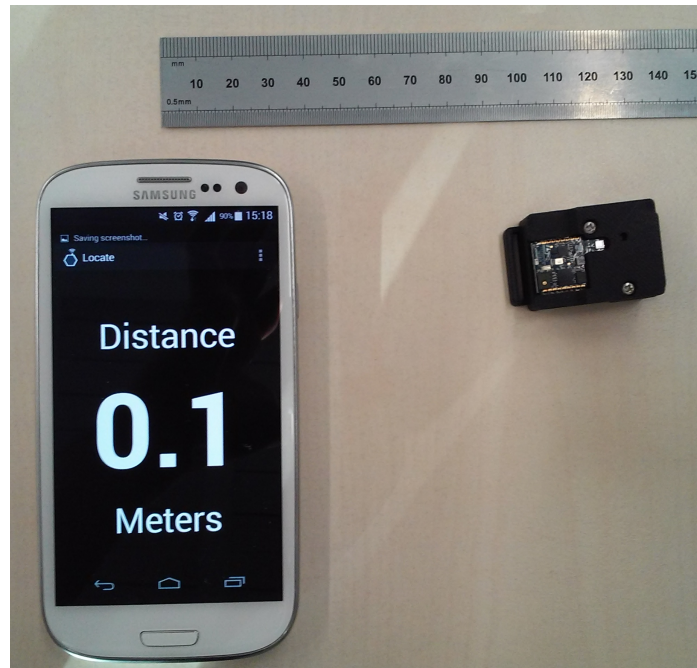


Figure 2.34: *SensorTile* used as Beacon. The App used on the Android device is Locate and can estimate the distance from the Beacon

## 2.5 Conclusions

This chapter showed the design of an innovative miniaturized wireless motion sensor, called *SensorTile*. The platform has met the requirements collected from customers for a reference design to start their projects. The module-shape in a 13.5 mm X 13.5 mm size only and the availability of a wide number of wired communication bus with the Bluetooth Low-Energy connectivity allows the *SensorTile* to be used as a sensor hub also. Without any modification, it can be used as a solderable module with a valid (limited) FCC certification.

The characterization of the antenna showed that the matching has been correctly performed and despite the gain is not very high, it is the maximum achievable with a chip antenna mounted on a PCB with a ground plane shorter than the wavelength of the RF signal.

Compare to the state of the art, this project:

1. It the smallest solderable sensor hub platform with Bluetooth radio connectivity, with